

Robust Graph Learning Against Adversarial Evasion Attacks via Prior-Free Diffusion-Based Structure Purification

Jiayi Luo
luojy@buaa.edu.cn
SKLCCSE, School of Computer
Science and Engineering
Beihang University
Beijing, China

Qingyun Sun*
sunqy@buaa.edu.cn
SKLCCSE, School of Computer
Science and Engineering
Beihang University
Beijing, China

Haonan Yuan
yuanhn@buaa.edu.cn
SKLCCSE, School of Computer
Science and Engineering
Beihang University
Beijing, China

Xingcheng Fu
fuxc@gxnu.edu.cn
Key Lab of Education Blockchain and
Intelligent Technology
Guangxi Normal University
Guangxi, China

Jianxin Li
lijx@buaa.edu.cn
SKLCCSE, School of Computer
Science and Engineering
Beihang University
Beijing, China

Abstract

Adversarial evasion attacks pose significant threats to graph learning, with lines of studies that have improved the robustness of Graph Neural Networks (GNNs). However, existing works rely on priors about clean graphs or attacking strategies, which are often heuristic and inconsistent. To achieve robust graph learning over different types of evasion attacks and diverse datasets, we investigate this problem from a prior-free structure purification perspective. Specifically, we propose a novel **Diff**usion-based **Str**ucture **Purification** framework named **DiffSP**, which creatively incorporates the graph diffusion model to learn intrinsic distributions of clean graphs and purify the perturbed structures by removing adversaries under the direction of the captured predictive patterns without relying on priors. DiffSP is divided into the forward diffusion process and the reverse denoising process, during which structure purification is achieved. To avoid valuable information loss during the forward process, we propose an LID-driven non-isotropic diffusion mechanism to selectively inject noise anisotropically. To promote semantic alignment between the clean graph and the purified graph generated during the reverse process, we reduce the generation uncertainty by the proposed graph transfer entropy guided denoising mechanism. Extensive experiments demonstrate the superior robustness of DiffSP against evasion attacks.

CCS Concepts

• **Mathematics of computing** → **Graph algorithms**; • **Networks** → **Network architectures**.

*Corresponding author.



This work is licensed under a Creative Commons Attribution 4.0 International License. *WWW '25, Sydney, NSW, Australia*
© 2025 Copyright held by the owner/author(s).
ACM ISBN 979-8-4007-1274-6/25/04
<https://doi.org/10.1145/3696410.3714815>

Keywords

robust graph learning, adversarial evasion attack, graph structure purification, graph diffusion

ACM Reference Format:

Jiayi Luo, Qingyun Sun, Haonan Yuan, Xingcheng Fu, and Jianxin Li. 2025. Robust Graph Learning Against Adversarial Evasion Attacks via Prior-Free Diffusion-Based Structure Purification. In *Proceedings of the ACM Web Conference 2025 (WWW '25)*, April 28-May 2, 2025, Sydney, NSW, Australia. ACM, New York, NY, USA, 13 pages. <https://doi.org/10.1145/3696410.3714815>

1 Introduction

Graphs are essential for modeling relationships in the social networks [69], recommendation systems [54], financial transactions [7], etc. While Graph Neural Networks (GNNs) [28] have advanced this field, concerns about their robustness have arisen [26, 66, 70]. Studies show that GNNs are vulnerable to evasion attacks [46], particularly structural perturbations [66, 71] where tiny changes to the graph topology can lead to a sharp performance decrease.

A wide range of works have been proposed to enhance graph robustness, categorizing into: 1) *Structure Learning Based* methods [11, 22, 67] that focus on refining graph structures; 2) *Preprocessing Based* methods [13, 52] that focus on denoising graphs during preprocessing stage; 3) *Robust Aggregation Based* methods [6, 17, 48, 70] that modify the aggregation process; and 4) *Adversarial Training Based* methods [58] that trains GNNs with adversarial samples. However, most approaches heavily depend on priors regarding clean graphs or attack strategies [22]. For example, the homophily prior [23, 25, 64, 67] and the low-rank prior [13, 26, 35, 57] are among the most commonly used assumptions. Unfortunately, when node features are unavailable, measuring the feature similarity becomes infeasible [22]. Additionally, imposing low-rank constraints risks discarding information encoded in the small singular values [11]. These prior-dependent limitations significantly hinder the ability of existing methods to achieve the universal robustness in graph learning across diverse scenarios.

To achieve prior-free robustness, we aim to adaptively learn the intrinsic distribution from clean graphs, which capture the underlying correlation and predictive patterns to enhance the robustness

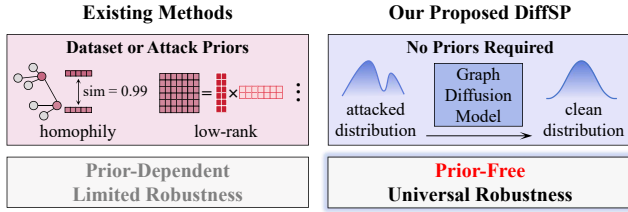


Figure 1: Comparison of existing robust GNNs and DiffSP. Existing robust GNNs rely on priors that limit adaptability, while DiffSP is prior-free with universal robustness.

of GNNs when facing unseen samples. Driven by this goal, we model the clean graph as a probability distribution over nodes and edges, encapsulating their predictable properties [33]. Attacks are disruptions to underlying distribution, causing it to shift away from the clean distribution [30]. To learn the latent distribution of clean graphs, diffusion models [39, 49] are an ideal choice, as shown in Figure 1. Instead of relying on priors, they model the implicit distributions in a data-centric manner, remaining agnostic to the dataset and attack strategies. Unlike other generative models, the “noising-denoising” process of graph diffusion models is well-suited to our goal. When encountering an attacked graph, the trained graph diffusion model gradually injects noise to obscure adversarial information during the forward process. In the reverse process, step-wise denoising enables removing both the adversarial information and injected noise, achieving prior-free graph purification.

Nevertheless, it still faces two significant challenges: 1) *How can we accurately identify and remove adversarial perturbations without disrupting the unaffected portions of the graph?* Evasion attacks typically involve subtle perturbations, making these alterations difficult to detect [46]. During the forward process, the isotropic indiscriminate noise affects both the normal and adversarial nodes, leading to excessive perturbations that can overmodify the graph. As a result, essential information may be lost, complicating the recovery of the clean structure during the reverse denoising phase. 2) *How can we ensure that the purified graph preserves the same semantics as the target clean graph?* The generation process in diffusion models involves repeated sampling from the distribution, with the inherent randomness promoting the creation of diverse graph samples. While this diversity can be beneficial in other domains of research, it poses a significant challenge to our task. Our objective is not to produce varied graphs, but to accurately recover the clean graph. Consequently, even if adversarial perturbations are successfully removed, there remains a risk that the purified graph may fail to semantically align with the target clean graph.

To address these challenges, we propose a novel **Diff**usion-based **Structure Purification** framework named **DiffSP**, which creatively incorporates the diffusion model to learn the intrinsic latent distributions of clean graphs and purify the perturbed structures by removing adversaries under the direction of the captured predictive patterns without relying on any priors. To remove adversaries while preserving the unaffected parts (\triangleright *Challenge 1*), we propose an LID-driven non-isotropic diffusion mechanism to selectively inject controllable noise anisotropically. By utilizing this non-isotropic noise, DiffSP effectively drowns out adversarial perturbations with minimal impact on normal nodes. To promote semantic alignment between the clean graph and the purified graph generated during

the reverse process (\triangleright *Challenge 2*), we reduce the generation uncertainty by the proposed graph transfer entropy guided denoising mechanism. Specifically, we maximize the transfer entropy between successive time steps during the reverse denoising process. This reduces uncertainty, stabilizes the graph generation, and guides the process toward achieving accurate graph purification. The main contributions of this paper are as follows:

- We propose DiffSP, a novel framework for adversarial graph purification against adversarial evasion attacks. To the best of our knowledge, this is the first prior-free robust graph learning framework by incorporating the graph diffusion model.
- We design an LID-driven non-isotropic forward diffusion process combined with a transfer entropy guided reverse denoising process, enabling precise removal of adversarial information while guiding the generation process toward target graph purification.
- Extensive experiments on both graph and node classification tasks on nine real-world datasets demonstrate the superior robustness of DiffSP against nine types of evasion attacks.

2 Related Work

Robust Graph Learning. Various efforts have been made to improve the robustness of graph learning against adversarial attacks, which can be grouped into four categories. 1) *Structure Learning Based* methods [11, 22, 26, 67] adjust the graph structure by removing unreliable edges or nodes to improve robustness. ProGNN [26] uses low-rank and smoothness regularization, GARNET [11] employs probabilistic models to learn a reduced-rank topology, GSR [67] leverages contrastive learning for structure refinement, and SG-GSR [22] addresses structural loss and node imbalance. 2) *Preprocessing Based* methods [13, 52] modify the graph before training. SVDGCN [13] retains top-k singular values from the adjacency matrix, while JaccardGCN [52] prunes adversarial edges based on Jaccard similarity. 3) *Robust Aggregation Based* methods [6, 17, 48, 70] improve the aggregation process to reduce sensitivity to adversarial perturbations. PA-GNN [48] and RGCN [70] use attention mechanisms to downweight adversarial edges, while Median [6] and Soft-Median [17] apply robust aggregation strategies to mitigate the effect of noisy features. 4) *Adversarial Training Based* methods [58] incorporate adversarial examples during training using min-max optimization to enhance resistance to attacks.

Graph Diffusion Models. Diffusion models have achieved significant success in graph generation tasks. Early works [27, 39] extended stochastic differential equations to graphs, but faced challenges due to the discrete nature of graphs. Graph structured diffusion [18, 49] addressed this by adapting D3PM [3], improving the quality and efficiency of graph generation. In addition, HypDiff [15] introduced a geometrically-based framework that preserves non-isotropic graph properties. To enhance scalability, EDGE [8] promotes sparsity by setting the empty graph as the target distribution. GraphMaker [31] further improved graph quality by applying asynchronous denoising to adjacency matrix and node features. However, directly applying existing graph diffusion models fails to achieve our goal because the indiscriminate noise risks damaging clean nodes. Additionally, the diversity of the graph diffusion model may lead to generated graphs that fit the clean distribution but have semantic information that differs from the target clean graph.

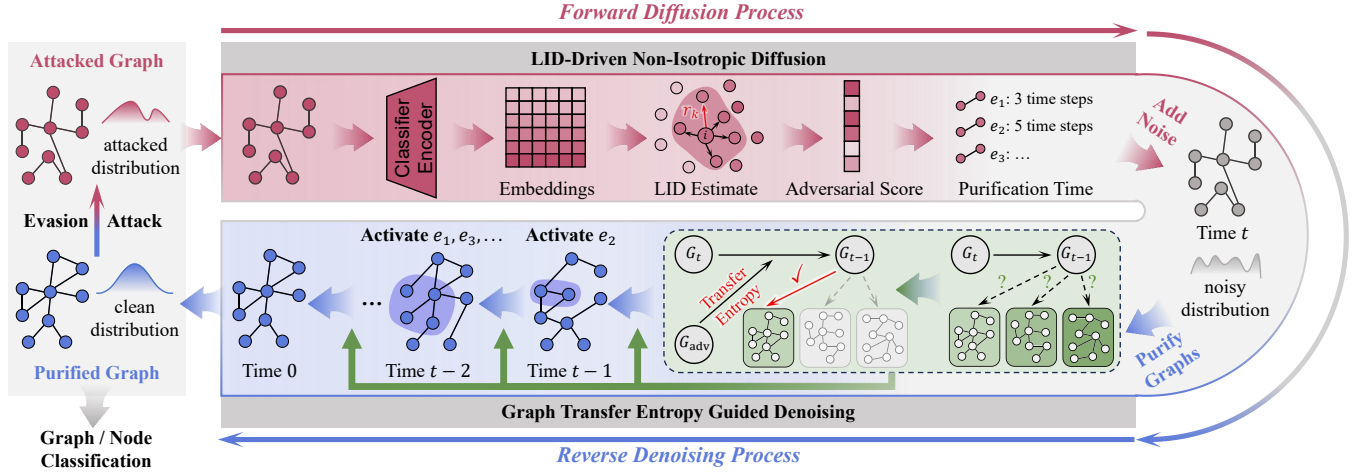


Figure 2: The overall architecture of DiffSP. DiffSP first employs a diffusion model to learn the predictive patterns of clean graphs. Then for the adversarial graph under evasion attack: 1) DiffSP injects non-isotropic noise by adjusting the diffusion time for each edge based on its adversarial degree, determined by LID. 2) During the generation process, DiffSP reduces uncertainty and guides the generation toward the target clean graph by maximizing the transfer entropy between two successive time steps.

3 Notations and Problem Formulation

In this work, we focus on enhancing robustness against adversarial evasion attacks with more threatening structural perturbation [71], where attackers perturb graph structures during the test phase, after the GNNs have been fully trained on clean datasets [5]. We represent a graph as $G = (X, A)$, where X is the node features and A is the adjacency. An attacked graph is denoted as $G_{\text{adv}} = (X, A_{\text{adv}})$, where A_{adv} is the perturbed adjacency matrix. Let c_θ be the GNN classifier trained on clean graph samples, and $\mathcal{D}_{\text{test}} = \{(\hat{s}_j, y_j)\}_{j=1}^M$ represent M attacked samples, where each \hat{s}_j is a graph or a node, and y_j is the corresponding label. The attacker’s goal is to maximize the number of misclassified samples, formulated as $\max \sum_{j=1}^M \mathbb{I}(c_\theta(\hat{s}_j) \neq y_j)$, by perturbing up to ϵ edges, where ϵ is constrained by the attack budget Δ . Our objective is to purify the attacked graph, reducing the effects of adversarial perturbations, and reinforcing the robustness of the GNNs to enhance the performance of downstream tasks.

4 DiffSP

In this section, we introduce our proposed framework named DiffSP which purifies the graph structure based on the learned predictive patterns without relying on any priors about the dataset or attack strategies. The overall architecture of DiffSP is shown in Figure 2. We first present our graph diffusion purification model which serves as the backbone of DiffSP, followed by detailing the two core components: the LID-Driven Non-Isotropic Diffusion Mechanism and the Graph Transfer Entropy Guided Denoising Mechanism.

4.1 Graph Diffusion Purification Model

For the backbone of DiffSP, we incorporate the structured diffusion model [3, 31, 49], which has shown to better preserve graph sparsity while reducing computational complexity [18, 49]. Since we focus on the more threatening structural perturbations [71], we exclude node features from the diffusion process and keep them fixed. Specifically, the noise in the forward process is represented by

a series of transition matrices, *i.e.*, $[\mathbf{Q}_A^{(1)}, \mathbf{Q}_A^{(2)}, \dots, \mathbf{Q}_A^{(T)}]$, where $(\mathbf{Q}_A^{(t)})_{ij}$ denotes the probability of transitioning from state i to state j for an edge at time step t . The forward Markov diffusion process is defined as $q(\mathbf{A}^{(t)} | \mathbf{A}^{(0)}) = \mathbf{A}^{(0)} \mathbf{Q}_A^{(1)} \dots \mathbf{Q}_A^{(t-1)} = \mathbf{A}^{(0)} \tilde{\mathbf{Q}}_A^{(t-1)}$. Here we utilize the marginal distributions of the edge state [49] as the noise prior distribution, thus $\tilde{\mathbf{Q}}_A^{(t)}$ can be expressed as $\tilde{\mathbf{Q}}_A^{(t)} = \bar{\alpha}^{(t)} \mathbf{I} + (1 - \bar{\alpha}^{(t)}) \mathbf{1} \mathbf{m}_A^\top$, where \mathbf{m}_A is the marginal distribution of edge states, $\bar{\alpha}^{(t)} = \cos^2(\frac{t/T+s}{1+s} \cdot \frac{\pi}{2})$ follows the cosine schedule [38] with a small constant s , \mathbf{I} is the identity matrix, and $\mathbf{1}$ is a vector of ones. During the reverse denoising process, we use the transformer convolution layer [42] as the denoising network $\phi(\cdot)_\theta$, trained for one-step denoising $p_\theta(\mathbf{A}^{(t-1)} | \mathbf{A}^{(t)}, t)$. We can train the denoising network to predict $\mathbf{A}^{(0)}$ instead of $\mathbf{A}^{(t-1)}$ since the posterior $q(\mathbf{A}^{(t-1)} | \mathbf{A}^{(t)}, \mathbf{A}^{(0)}, t) \propto \mathbf{A}^{(t)} (\mathbf{Q}_A^{(t)})^\top \odot \mathbf{A}^{(0)} \tilde{\mathbf{Q}}_A^{(t-1)}$ has a closed form expression [31, 44, 45], where \odot is the Hadamard product. Once trained, we can generate graphs by iteratively applying $\phi(\cdot)_\theta$.

4.2 LID-Driven Non-Isotropic Diffusion Mechanism

Adversarial attacks typically target only a small subset of nodes or edges to fool the GNNs while remaining undetected. Injecting isotropic noise uniformly across all nodes, which means applying the same level of noise to each node regardless of its individual characteristics [50], poses a significant challenge. While isotropic noise can effectively drown out adversarial perturbations during the forward diffusion process, it inevitably compromises the clean and unaffected portions of the graph. As a result, both the adversarial and the valuable information are erased, making purification during the reverse denoising process more difficult.

To remove the adversarial perturbations without losing valuable information, we design a novel LID-Driven Non-Isotropic Diffusion Mechanism. The core idea is to inject more noise into adversarial nodes identified by Local Intrinsic Dimensionality (LID) while

minimizing disruption to clean nodes. In practice, the noise level associated with different edges is distinct and independent. As a result, the noise associated with each edge during the forward diffusion process is represented by an independent transition matrix. The adjacency matrix $\mathbf{A}^{(t)}$ at time step t is then updated as follows:

$$\mathbf{A}_{ij}^{(t)} = \mathbf{A}_{ij}(\bar{\mathbf{Q}}_{\mathbf{A}}^{(t)})_{ij}, \quad (1)$$

$$(\bar{\mathbf{Q}}_{\mathbf{A}}^{(t)})_{ij} = \bar{\alpha}^{(t)}\mathbf{I} + (\Lambda_{\mathbf{A}})_{ij}(1 - \bar{\alpha}^{(t)})\mathbf{1}\mathbf{m}_{\mathbf{A}}^{\top}, \quad (2)$$

where $\Lambda_{\mathbf{A}} \in \mathbb{R}^{N \times N}$ represents the adversarial degree of each edge.

Based on the above analysis, locating the adversarial information and determining the value of $\Lambda_{\mathbf{A}}$ is crucial for effective adversarial purification. Local Intrinsic Dimensionality (LID) [21, 37] measures the complexity of data distributions around a reference point o by assessing how quickly the number of data points increases as the distance from the reference point expands. Let $F(r)$ denote the cumulative distribution function of the distances between the reference point o and other data points at distance r and $F(r)$ is positive and differentiable at $r \geq 0$, the LID of point o at distance r is defined as $\lim_{\epsilon \rightarrow 0} \frac{\ln F((1+\epsilon)r)/F(r)}{\ln(1+\epsilon)}$ [21]. According to the manifold hypothesis [14], each node n_i in a graph lies on a low-dimensional natural manifold S . Adversarial nodes being perturbed will deviate from this natural data manifold S , leading to an increase in LID [37], which can quantify the dimensionality of the local data manifold. Therefore, we use LID to measure the adversarial degree, $\Lambda_{\mathbf{A}}$. Higher LID values indicate that the local manifold around a node has expanded beyond its natural low-dimensional manifold S , signaling the presence of adversarial perturbations. In this work, we use the Maximum Likelihood Estimator (MLE) [2] to estimate the LID value of graph nodes, providing a useful trade-off between statistical efficiency and computational complexity [37]. Specifically, let $\Gamma \in \mathbb{R}^n$ represent the vector of estimated LID values, where Γ_i denotes the LID value of node n_i , which is estimated as follows:

$$\Gamma_i = - \left(\frac{1}{k} \sum_{j=1}^k \log \frac{r_j(n_i)}{r_k(n_i)} \right)^{-1}. \quad (3)$$

Here, $r_j(n_i)$ represents the distance between node n_i and its j -th nearest neighbor n_i^j . Based on the observation that the deeper layers of a neural network reveal more linear and “unwrapped” manifolds compared to the input space [16], we compute the $r_j(n_i)$ as the Euclidean distance [12] between the hidden features of two nodes in the last hidden layer of the trained GNN classifier $c(\cdot)_{\theta}$. After obtaining the LID values vector Γ , we can calculate $\Lambda_{\mathbf{A}} = \Gamma\Gamma^{\top}$.

However, in practice, using the non-isotropic transition matrix in Eq. (1) requires the diffusion model to predict the previously injected non-isotropic noise during the reverse process. This task is more challenging because, unlike isotropic noise, non-isotropic noise varies across different edges. As a result, the model must learn to predict various noise distributions that are both spatially and contextually dependent on the graph structure and node features. This increases the difficulty of accurately estimating and removing the noise across graph regions, making the reverse denoising process significantly more intricate. Moreover, training the model to develop the ability to inject more noise into adversarial perturbations and remove it during the reverse process relies on having access to adversarial training data. However, in the evasion attack

settings, where the model lacks access to adversarial graphs during training, its ability to achieve precise non-isotropic denoising is limited. Inspired by [63], we introduce the following proposition:

PROPOSITION 1. *For each edge at time t , the adjacency matrix is updated as $\mathbf{A}_{ij}^{(t)} = \mathbf{A}_{ij}(\bar{\mathbf{Q}}_{\mathbf{A}}^{(t)})_{ij}$, where the non-isotropic transition matrix is $(\bar{\mathbf{Q}}_{\mathbf{A}}^{(t)})_{ij} = \bar{\alpha}^{(t)}\mathbf{I} + (\Lambda_{\mathbf{A}})_{ij}(1 - \bar{\alpha}^{(t)})\mathbf{1}\mathbf{m}_{\mathbf{A}}^{\top}$. There exists a unique time $\hat{t}(\mathbf{A}_{ij}) \in [0, T]$ such that $(\bar{\mathbf{Q}}_{\mathbf{A}}^{(t)})_{ij} \Leftrightarrow (\bar{\mathbf{Q}}_{\mathbf{A}}^{\hat{t}(\mathbf{A}_{ij})})_{ij}$, where:*

$$\hat{t}(\mathbf{A}_{ij}) = T \left(\frac{2(1+s)}{\pi} \cos^{-1} \left(\sqrt{\frac{\bar{\alpha}^{(t)}}{(\Lambda_{\mathbf{A}})_{ij}(1 - \bar{\alpha}^{(t)}) + \bar{\alpha}^{(t)}}}} \right) - s \right). \quad (4)$$

This proposition demonstrates that non-isotropic noise can be mapped to isotropic noise by adjusting the diffusion times accordingly. The detailed proof is provided in Appendix A.1. Building on this proposition, we bypass the need to train a diffusion model that can predict non-isotropic noise in the reverse denoising process. Instead, we handle the need for non-isotropic noise injection by applying isotropic noise uniformly to all edges, while varying the total diffusion time for each edge. By controlling the diffusion time for each edge, we can effectively manage the noise introduced to each node, ensuring that the injected noise accounts for the adversarial degree of each node. Let $\hat{\mathbf{A}}^{(t) \prime}$ represents the adjacency matrix at time t during the reverse denoising process, we have:

$$\hat{\mathbf{A}}^{(t) \prime} = \mathbf{M}^{(t)} \odot \hat{\mathbf{A}}^{(t)} + (1 - \mathbf{M}^{(t)}) \odot \mathbf{A}^{(t)}, \quad (5)$$

where $\hat{\mathbf{A}}^{(t)}$ is the adjacency matrix predicted by $\phi(\cdot)_{\theta}$, $\mathbf{A}^{(t)}$ is the noisy adjacency matrix obtained by $\mathbf{A}^{(t)} = \mathbf{A}\bar{\mathbf{Q}}_{\mathbf{A}}^{(t)}$ in the forward diffusion process, and $\mathbf{M}^{(t)}$ is the binary mask matrix that indicates which edges are being activated to undergo purification at time step t , achieving the non-isotropic diffusion. $\mathbf{M}_{ij}^{(t)}$ is defined as:

$$\mathbf{M}_{ij}^{(t)} = \begin{cases} 0, & t > \hat{t}(\mathbf{A}_{ij}) \\ 1, & t \leq \hat{t}(\mathbf{A}_{ij}) \end{cases}, \quad (6)$$

where $\hat{t}(\mathbf{A}_{ij})$ is obtained according to Proposition 1. This implies that clean nodes are not denoised until the specified time. In this way, adversarial information receives sufficient denoising, while valuable information is not subjected to excessive perturbations.

4.3 Graph Transfer Entropy Guided Denoising Mechanism

In structured diffusion models [3], the reverse process involves multiple rounds of sampling from the distribution, which introduces inherent randomness. This randomness is useful for generating diverse graph samples but creates challenges for our purification goal. During the reverse denoising process, the diversity of diffusion can result in purified graphs that, although free from adversarial attacks and fit the clean distribution, deviate from the target graph and have different ground truth labels. This presents a significant challenge: we not only encourage the generated graph to be free from adversarial information but also aim for it to retain the same semantic information as the target clean graph.

To address this challenge, we introduce a Graph Transfer Entropy Guided Denoising Mechanism to minimize the generation uncertainty in the reverse Markov chain $\langle \hat{G}^{(T-1)} \rightarrow \hat{G}^{(T-2)} \rightarrow$

$\dots \rightarrow \hat{G}^{(0)}$). Transfer entropy [40] is a non-parametric statistic that quantifies the directed transfer of information between random variables. The transfer entropy from $\hat{G}^{(t)}$ to $\hat{G}^{(t-1)}$ in the reverse process by knowing the adversarial graph G_{adv} , can be defined in the form of conditional mutual information [56]:

$$I(\hat{G}^{t-1}; G_{\text{adv}} | \hat{G}_t) = H(\hat{G}^{(t-1)} | \hat{G}^{(t)}) - H(\hat{G}^{(t-1)} | \hat{G}^{(t)}, G_{\text{adv}}), \quad (7)$$

where $I(\cdot)$ represents mutual information and $H(\cdot)$ is the Shannon entropy. This measures the uncertainty reduced about future value $\hat{G}^{(t-1)}$ conditioned on the value G_{adv} , given the knowledge of past values $\hat{G}^{(t)}$. Given the unnoticeable characteristic of adversarial attacks, which typically involve only small perturbations to critical edges without altering the overall semantic information of most nodes, the target clean graph has only minimal differences from G_{adv} . Therefore, by increasing the $I(\hat{G}^{t-1}; G_{\text{adv}} | \hat{G}_t)$, we can mitigate the negative impacts of generative diversity on our goal and guide the direction of the denoising process, ensuring that the generation towards the target clean graph. Specifically, the purified graph will not only be free from adversarial attacks but will also share the same semantic information as the target clean graph. However, calculating Eq. (7) requires estimating both the entropy and joint entropy of graph data, which remains an open problem.

In this work, we propose a novel method for estimating graph entropy and joint entropy. Let z_i be the representations of node n_i after message passing. By treating the set $\mathcal{Z} = \{z_1, z_2, \dots, z_n\}$ as a collection of variables that capture both feature and structure information of the graph, we approximate it as containing the essential information of the graph. From this perspective, the entropy of the graph can be estimated using matrix-based Rényi α -order entropy [62], which provides an insightful approach to calculating the graph entropy. Specifically, let \mathbf{K} denote the Gram matrix obtained from evaluating a positive definite kernel k on all pairs of z with $\mathbf{K}_{ij} = \exp\left(-\frac{\|z_i - z_j\|^2}{2\sigma^2}\right)$, where σ is a hyperparameter selected follows the Silverman's rule [43], the graph entropy can then be defined as the Rényi's α -order entropy $S_\alpha(\cdot)$ [62]:

$$H(G) = S_\alpha(\hat{\mathbf{K}}) = \frac{1}{1-\alpha} \log \left[\sum_1^n \lambda_i^\alpha(\hat{\mathbf{K}}) \right], \quad (8)$$

where $\hat{\mathbf{K}}_{ij} = \frac{\mathbf{K}_{ij}}{\sqrt{\mathbf{K}_{ii}\mathbf{K}_{jj}}}$, $\lambda_i(\hat{\mathbf{K}})$ denotes the i -th eigenvalue of $\hat{\mathbf{K}}$, and α is a task-dependent parameter [62]. In the context of graph learning, Eq. (8) captures the characteristics of the graph's community structure: lower graph entropy signifies a more cohesive and well-defined community structure, whereas higher graph entropy indicates a more disordered and irregular arrangement. Further details can be found in Appendix B. For a collection of m graphs with their node representations after message passing $\{\mathcal{Z}_i = (z_1^i, z_2^i, \dots, z_n^i)\}_{i=1}^m$, the joint graph entropy is defined as [62]:

$$H(G_1, G_2, \dots, G_m) = S_\alpha \left(\frac{\hat{\mathbf{K}}_1 \odot \hat{\mathbf{K}}_2 \odot \dots \odot \hat{\mathbf{K}}_m}{\text{tr}(\hat{\mathbf{K}}_1 \odot \hat{\mathbf{K}}_2 \odot \dots \odot \hat{\mathbf{K}}_m)} \right), \quad (9)$$

where $\hat{\mathbf{K}}_i$ is the normalized Gram matrix of G_i , \odot represents the Hadamard product, and $\text{tr}(\cdot)$ is the matrix trace. Further understanding of our calculation method can be found in Appendix B.

By combining Eq. (8) and Eq. (9), we can get the value of transfer entropy $I(\hat{G}^{(t-1)}; G_{\text{adv}} | \hat{G}^{(t)})$. The detailed derivation process is

provided in Appendix A.2. Intuitively, based on our entropy estimation method, maximizing $I(\hat{G}^{(t-1)}; G_{\text{adv}} | \hat{G}^{(t)})$ will guide the node entanglement of the generated $\hat{G}^{(t-1)}$ towards that of G_{adv} , preventing the reverse denoising process from deviating from the target direction. To achieve this, we update the generation process using the negative gradient of $I(\hat{G}^{(t-1)}; G_{\text{adv}} | \hat{G}^{(t)})$ concerning $\hat{\mathbf{A}}^{(t-1)}$:

$$\hat{\mathbf{A}}^{(t-1)} \leftarrow \hat{\mathbf{A}}^{(t-1)} + \lambda \nabla_{\hat{\mathbf{A}}^{(t-1)}} I(\hat{G}^{(t-1)}; G_{\text{adv}} | \hat{G}^{(t)}), \quad (10)$$

where λ is a hyperparameter controlling the guidance scale. Early in the denoising process, maximizing the $I(\hat{G}^{(t-1)}; G_{\text{adv}} | \hat{G}^{(t)})$ will steer the overall direction of the generation toward better purification. However, as the graph becomes progressively cleaner, maintaining the same level of guidance could cause the re-emergence of adversarial information in the generated graph. Therefore, it is essential to adjust the guidance scale dynamically over time. We propose that the scale of guidance should depend on the ratio between the injected noise and the adversarial perturbation at each time step. We update the guidance process in Eq. (10) as follows:

$$\hat{\mathbf{A}}^{(t-1)} \leftarrow \hat{\mathbf{A}}^{(t-1)} - \frac{\lambda}{1-\alpha} \nabla_{\hat{\mathbf{A}}^{(t-1)}} I(\hat{G}^{(t-1)}; G_{\text{adv}} | \hat{G}^{(t)}). \quad (11)$$

4.4 Training Pipeline of DiffSP

Under the adversarial evasion structural attacks, we train the proposed DiffSP along with the classifier using the overall objective loss function $\mathcal{L} = \mathcal{L}_{\text{cls}} + \mathcal{L}_{\text{diff}}$, where:

$$\mathcal{L}_{\text{cls}} = \text{cross-entropy}(\hat{y}, y), \quad (12)$$

$$\mathcal{L}_{\text{diff}} = \mathbb{E}_{q(\mathbf{A}^{(0)})} \mathbb{E}_{q(\mathbf{A}^t | \mathbf{A}^{(0)})} \left[-\log p_\theta(\mathbf{A}^{(0)} | \mathbf{A}^{(t)}, t) \right]. \quad (13)$$

The classifier loss \mathcal{L}_{cls} measures the difference between the predicted label \hat{y} and the ground truth y . The graph diffusion model loss $\mathcal{L}_{\text{diff}}$ accounts for the reverse denoising process [3]. Initially, we train the classifier, followed by the independent training of the diffusion model. Once both models are trained, they are used together to purify adversarial graphs. The training pipeline of DiffSP is detailed in Algorithm 1, and complexity analysis is in Appendix C.

Algorithm 1: Overall training pipeline of DiffSP.

Input: Evasion attacked graph $G_{\text{adv}} = (\mathbf{X}, \mathbf{A}_{\text{adv}})$; Classifier $c(\cdot)_\theta$; Graph diffusion purification model $\phi(\cdot)_\theta$; Hyperparameters $T, k, \lambda, \sigma, \alpha, \eta$.

Output: Purified graph $\hat{G} = (\mathbf{X}, \hat{\mathbf{A}})$; Learned parameter $\hat{\theta}$.

- 1 Update by back-propagation $\hat{\theta} \leftarrow \hat{\theta} - \eta \nabla_{\hat{\theta}} \mathcal{L}$;
// LID-Driven Non-Isotropic Diffusion
 - 2 Assess node adversarial degree Γ based on LID \leftarrow Eq. (3);
 - 3 Calculate the edge adversarial degree $\Lambda_{\mathbf{A}} = \Gamma \Gamma^T$;
 - 4 Obtain the purification time of each edge $\hat{t}(\mathbf{A}_{ij}) \leftarrow$ Eq. (4);
 - 5 **for** $t = T, T-1, \dots, 1$ **do**
 - 6 Establish the purification mask $\mathbf{M}^{(t-1)} \leftarrow$ Eq. (6);
 - 7 Execute one step denoising $\hat{\mathbf{A}}^{(t-1)} \leftarrow$ Eq. (5);
// Graph Transfer Entropy Guided Denoising
 - 8 Calculate the graph transfer entropy \leftarrow Eq. (7), (8), (9);
 - 9 Guide the reverse denoising process \leftarrow Eq. (11);
 - 10 Obtain the $\hat{\mathbf{A}}^{(0)}$ as the purified adjacency matrix $\hat{\mathbf{A}}$.
-

Table 1: Accuracy score (% \pm standard deviation) of graph classification task on real-world datasets against adversarial attacks. The best results are shown in bold type and the runner-ups are underlined. OOM indicates out-of-memory.

Dataset	Attack	GCN	IDGL	GraphCL	VIB-GSL	G-Mixup	SEP	MGRL	SCGCN	HSP-SL	SubGatPool	DIR	VGIB	DiffSP
MUTAG	GradArgmax	54.44 \pm 4.16	47.78 \pm 5.09	55.00 \pm 3.89	<u>69.45\pm2.78</u>	60.00 \pm 5.44	62.78 \pm 4.34	66.67 \pm 3.51	67.22 \pm 3.89	68.33 \pm 3.51	62.78 \pm 3.56	54.44 \pm 4.16	68.52 \pm 2.62	70.00\pm4.44
	PR-BCD	51.66 \pm 5.00	65.00 \pm 6.11	59.44 \pm 6.11	62.77 \pm 4.34	<u>71.11\pm3.33</u>	55.00 \pm 9.44	56.67 \pm 4.16	63.89 \pm 2.78	65.56 \pm 2.22	65.56 \pm 5.98	52.77 \pm 6.21	57.78 \pm 3.68	72.77\pm6.31
	CAMA	40.56 \pm 2.54	73.89\pm2.55	44.26 \pm 3.80	59.34 \pm 3.52	60.00 \pm 2.22	60.56 \pm 1.67	39.45 \pm 1.67	64.45 \pm 7.11	43.33 \pm 2.22	66.11 \pm 5.80	62.22 \pm 8.17	61.67 \pm 1.67	<u>68.33\pm9.31</u>
	Average	48.89	62.22	52.90	64.04	63.70	59.45	54.26	65.19	59.07	<u>64.82</u>	56.48	62.66	70.18
IMDB-B	GradArgmax	62.79 \pm 1.08	59.20 \pm 1.08	65.19 \pm 0.87	68.90 \pm 1.45	50.89 \pm 0.20	<u>72.00\pm1.55</u>	64.00 \pm 0.77	68.60 \pm 1.50	62.50 \pm 0.80	61.00 \pm 1.10	68.10 \pm 1.04	63.80 \pm 0.87	76.00\pm1.15
	PR-BCD	50.89 \pm 1.92	<u>71.39\pm1.91</u>	65.69 \pm 1.35	70.49 \pm 1.20	41.90 \pm 0.94	70.40 \pm 1.28	57.10 \pm 1.37	66.80 \pm 1.89	67.59 \pm 1.28	69.69 \pm 2.00	67.20 \pm 1.08	65.10 \pm 1.51	74.10\pm1.22
	CAMA	52.19 \pm 1.33	68.40 \pm 0.66	59.19 \pm 0.75	64.50 \pm 1.20	57.40 \pm 0.48	<u>69.20\pm0.98</u>	54.30 \pm 1.35	67.60 \pm 1.50	55.99 \pm 1.41	67.60 \pm 2.11	61.10 \pm 1.45	56.70 \pm 1.62	75.90\pm0.99
	Average	55.29	66.33	63.36	67.96	50.06	<u>70.53</u>	58.47	67.67	62.03	66.10	65.47	61.87	75.33
IMDB-M	GradArgmax	38.53 \pm 2.00	46.07 \pm 0.76	40.18 \pm 3.63	44.20 \pm 1.16	39.26 \pm 0.47	42.07 \pm 0.70	42.53 \pm 1.68	45.60 \pm 1.87	41.33 \pm 0.42	<u>47.43\pm0.79</u>	38.20 \pm 0.67	44.40 \pm 0.94	48.47\pm1.12
	PR-BCD	35.00 \pm 1.31	<u>46.00\pm1.46</u>	43.53 \pm 1.12	45.60 \pm 1.69	36.11 \pm 0.63	35.27 \pm 0.70	38.07 \pm 2.24	42.47 \pm 1.66	37.13 \pm 0.43	38.97 \pm 1.64	37.33 \pm 0.79	43.11 \pm 1.75	47.00\pm1.44
	CAMA	38.40 \pm 1.69	<u>46.27\pm0.33</u>	42.80 \pm 0.88	46.00 \pm 0.94	37.99 \pm 1.69	44.47 \pm 0.99	41.00 \pm 1.50	45.67 \pm 2.12	41.13 \pm 1.23	43.56 \pm 0.60	39.73 \pm 1.74	38.87 \pm 1.46	48.13\pm2.44
	Average	37.31	<u>46.11</u>	42.17	45.27	37.79	40.60	40.53	44.58	39.86	43.32	38.42	42.13	47.87
REDDIT-B	GradArgmax	40.24 \pm 0.51		55.16 \pm 0.87	52.25 \pm 0.51	40.84 \pm 0.22	<u>66.95\pm2.70</u>	66.40 \pm 0.49	64.40 \pm 1.88	62.90 \pm 0.76	59.80 \pm 0.78	54.00 \pm 0.32	57.35 \pm 0.74	67.35\pm0.55
	PR-BCD	51.82 \pm 1.09	OOM	51.96 \pm 0.57	57.06 \pm 1.55	55.05 \pm 1.55	54.85 \pm 1.94	51.65 \pm 0.32	52.05 \pm 1.78	<u>64.20\pm1.94</u>	66.00 \pm 3.29	56.15 \pm 1.29	54.05 \pm 0.35	67.63\pm0.42
	CAMA	51.49 \pm 0.59		58.84 \pm 0.95	62.65 \pm 0.90	54.95 \pm 0.57	<u>66.50\pm3.02</u>	48.10 \pm 0.92	67.85 \pm 1.90	69.90\pm0.49	53.90 \pm 0.30	60.40 \pm 0.54	55.90 \pm 1.04	<u>68.15\pm0.95</u>
	Average	47.85	OOM	55.32	57.32	50.28	62.77	55.38	61.43	<u>65.67</u>	59.90	56.85	55.77	67.71
COLLAB	GradArgmax	59.30 \pm 1.37	66.84 \pm 0.83	62.08 \pm 0.59	<u>68.00\pm0.31</u>	51.49 \pm 0.50	62.86 \pm 1.19	52.88 \pm 0.45	54.83 \pm 1.12	58.68 \pm 0.39	62.62 \pm 0.74	62.98 \pm 0.52	61.10 \pm 1.00	68.08\pm0.78
	PR-BCD	46.74 \pm 0.70	<u>67.00\pm1.13</u>	57.40 \pm 1.67	66.52 \pm 0.88	56.08 \pm 1.19	53.38 \pm 1.90	44.34 \pm 1.46	49.46 \pm 1.17	53.00 \pm 0.60	61.02 \pm 0.97	64.30 \pm 0.48	57.04 \pm 0.67	67.56\pm0.69
	CAMA	49.70 \pm 1.04	67.92\pm0.20	62.08 \pm 0.59	66.96 \pm 0.56	48.38 \pm 0.60	60.21 \pm 1.01	54.14 \pm 0.41	54.90 \pm 1.07	56.60 \pm 0.37	56.92 \pm 0.61	62.86 \pm 0.47	59.64 \pm 0.46	<u>67.06\pm0.63</u>
	Average	51.91	<u>67.25</u>	60.52	67.16	51.98	58.82	50.45	53.06	56.09	60.19	63.38	59.26	67.57

5 Experiment

Datasets. We assess the robustness of DiffSP¹ in graph and node classification tasks. For graph classification, we use MUTAG [24], IMDB-BINARY [24], IMDB-MULTI [24], REDDIT-BINARY [24], and COLLAB [24]. For node classification, we test on Cora [59], CiteSeer [59], Polblogs [1], and Photo [41]. Details are in Appendix D.1.

Baselines. Due to the limited research on robust GNNs targeting graph classification, we compare DiffSP with robust representation learning and structure learning methods designed for graph classification, including IDGL [9], GraphCL [60], VIB-GSL [47], G-Mixup [20], SEP [53], MGRL [36], SCGCN [68], HSP-SL [65], SubGatPool [4] DIR [55], and VGIB [61]. For node classification, we choose baselines from: 1) *Structure Learning Based* methods, including GSR [67], GARNET [11], and GUARD [29]; 2) *Preprocessing Based* methods, including SVDGCN [13] and JaccardGCN [52]; 3) *Robust Aggregation Based* methods, including RGCN [70], MedianGCN [6], GNNGuard [64], SoftMedian [17], and ElasticGCN [34]; and 4) *Adversarial Training Based* methods, represented by the GraphADV [58]. Details of baselines can be found in Appendix D.2.

Adversarial Attack Settings. For graph classification, we evaluate the performance against three strong evasion attacks: PR-BCD [17], GradArgmax [10], and CAMA-subgraph [51]. For node classification, we evaluate six evasion attacks: 1) *Targeted Attacks*: PR-BCD [17], Nettack [71], and GR-BCD [17]; 2) *Non-targeted Attacks*: MinMax [32], DICE [72], and Random [32]. Further details on the attack methods and budget settings are provided in Appendix D.3.

Hyperparameter Settings. Details are provided in Appendix D.4.

5.1 Adversarial Robustness

Graph Classification Robustness. We evaluated the robustness of the graph classification task under three adversarial attacks across five datasets. Since the choice of classifier affects attack effectiveness, especially in graph classification due to pooling operations, it

is crucial to standardize the model architecture. Simple changes like adding a linear layer can reduce the impact of attacks. To ensure a fair comparison, we used a two-layer GCN with a linear layer and mean pooling for both the baselines and our proposed DiffSP. Each experiment was repeated 10 times, with results shown in Table 1.

Result. 1) DiffSP consistently outperforms all baselines under the PR-BCD attack and achieves the highest average robustness across all attacks on five datasets, with a notable 4.80% average improvement on the IMDB-BINARY dataset. 2) It’s important to note that while baselines may excel against specific attacks, they often struggle with others. In contrast, DiffSP maintains consistent robustness across both datasets and attacks, thanks to its ability to learn clean distributions and purify adversarial graphs without relying on specific priors about the dataset or attack strategies.

Node Classification Robustness. We evaluate the robustness of DiffSP on the node classification task against six attacks across four datasets, using the same other settings as in the graph classification experiments. The results are presented in Table 2 and Table 3.

Result. We have two key observations: 1) DiffSP achieves the best average performance across both targeted and non-targeted attacks on all datasets, demonstrating its robust adaptability across diverse scenarios. 2) DiffSP performs particularly well under stronger attacks but is less effective against weaker ones like Random and DICE. This is because these attacks introduce numerous noisy edges, many of which do not exhibit distinctly adversarial characteristics. Instead, these edges are often plausible within the graph. Consequently, these additional perturbations can mislead DiffSP, making it harder to discern the correct information within the graph, leading the generated graph to deviate from the target clean graph.

5.2 Ablation Study

In this subsection, we analyze the effectiveness of DiffSP’s two core components: 1) DiffSP (w/o LN), which excludes the LID-Driven Non-Isotropic Diffusion Mechanism; and 2) DiffSP (w/o TG), which excludes the Graph Transfer Entropy Guided Denoising Mechanism.

¹Our code is available at <https://github.com/RingBDStack/DiffSP>

Table 2: Accuracy score (% \pm standard deviation) of node classification task on real-world datasets against targeted attack.

Dataset	Attack	GCN	GSR	GARNET	GUARD	SVD	Jaccard	RGCN	MedianGCN	GNNGuard	SoftMedian	ElasticGCN	GraphAT	DiffSP
Cora	PR-BCD	55.59 \pm 1.47	74.75 \pm 0.53	66.80 \pm 0.46	65.71 \pm 0.79	64.66 \pm 0.35	60.49 \pm 1.00	55.91 \pm 0.65	61.77 \pm 0.68	65.14 \pm 1.07	59.36 \pm 0.63	63.86 \pm 1.38	63.74 \pm 0.99	75.13 \pm 1.27
	Nettack	49.25 \pm 5.28	67.25 \pm 5.20	62.95 \pm 4.75	52.50 \pm 4.08	70.25 \pm 0.79	56.75 \pm 2.65	47.50 \pm 1.67	76.25 \pm 5.17	76.00 \pm 5.03	67.50 \pm 4.25	65.25 \pm 3.22	73.50 \pm 9.14	77.75 \pm 3.62
	GR-BCD	66.34 \pm 1.45	78.86 \pm 0.53	72.35 \pm 0.91	72.08 \pm 1.23	65.34 \pm 0.72	71.88 \pm 0.76	69.74 \pm 2.08	72.90 \pm 1.06	70.45 \pm 1.20	75.52 \pm 0.86	78.44 \pm 1.42	77.06 \pm 1.24	76.83 \pm 0.65
	Average	57.06	73.62	67.37	63.43	66.75	63.04	57.72	70.31	70.53	67.46	69.18	71.43	76.57
CiteSeer	PR-BCD	45.06 \pm 1.83	63.33 \pm 0.60	55.75 \pm 1.71	54.48 \pm 0.96	59.61 \pm 0.51	48.72 \pm 1.20	41.08 \pm 1.55	49.72 \pm 0.71	49.78 \pm 2.33	49.20 \pm 0.89	48.79 \pm 1.41	61.54 \pm 1.01	64.35 \pm 0.89
	Nettack	60.75 \pm 8.34	75.25 \pm 2.65	72.00 \pm 2.84	59.25 \pm 3.92	77.25 \pm 1.84	71.50 \pm 3.16	42.25 \pm 4.78	74.00 \pm 2.93	77.00 \pm 3.50	59.00 \pm 2.11	63.50 \pm 3.76	73.25 \pm 5.14	78.80 \pm 4.53
	GR-BCD	50.56 \pm 2.17	65.50 \pm 0.57	57.04 \pm 2.57	54.74 \pm 1.82	60.40 \pm 0.59	59.83 \pm 1.17	44.82 \pm 1.60	55.17 \pm 1.31	58.88 \pm 3.38	55.65 \pm 0.93	60.37 \pm 2.91	62.25 \pm 1.25	65.63 \pm 1.30
	Average	52.12	68.02	61.60	56.16	65.75	60.02	42.72	59.63	61.89	54.62	57.55	65.68	69.59
PolBlogs	PR-BCD	73.73 \pm 1.19	86.50 \pm 0.52	75.52 \pm 0.50	81.82 \pm 1.06	78.02 \pm 0.16	51.45 \pm 1.23	74.01 \pm 0.32	65.07 \pm 4.21	51.93 \pm 2.54	87.88 \pm 1.29	74.71 \pm 2.89	80.67 \pm 0.85	90.24 \pm 0.92
	Nettack	74.75 \pm 4.92	75.75 \pm 1.69	83.75 \pm 3.77	76.75 \pm 3.13	80.75 \pm 1.69	47.75 \pm 6.06	76.50 \pm 1.75	46.00 \pm 2.11	50.24 \pm 6.52	83.50 \pm 3.37	86.00 \pm 4.12	83.95 \pm 2.72	84.55 \pm 5.90
	GR-BCD	71.31 \pm 3.41	84.75 \pm 0.66	75.49 \pm 0.77	87.13 \pm 3.63	90.27 \pm 0.36	50.71 \pm 1.98	79.13 \pm 0.54	56.95 \pm 5.15	51.26 \pm 1.78	87.50 \pm 0.81	91.12 \pm 2.71	92.70 \pm 0.18	92.75 \pm 0.38
	Average	73.26	82.33	78.25	81.90	83.01	49.97	76.55	56.01	51.14	86.29	83.94	85.77	89.18
Photo	PR-BCD	65.35 \pm 2.48	73.81 \pm 1.90	77.58 \pm 1.93	84.14 \pm 3.75	80.04 \pm 1.13	66.13 \pm 2.82	63.79 \pm 1.99	79.75 \pm 0.96	65.62 \pm 2.63	76.84 \pm 1.46	76.21 \pm 1.89	78.72 \pm 2.13	84.78 \pm 1.82
	Nettack	74.75 \pm 5.16	88.75 \pm 4.12	88.00 \pm 3.07	84.25 \pm 2.65	82.75 \pm 5.45	75.50 \pm 5.43	75.50 \pm 3.07	86.50 \pm 3.16	87.50 \pm 5.77	88.75 \pm 1.32	83.00 \pm 3.29	87.25 \pm 12.30	87.75 \pm 4.32
	GR-BCD	69.11 \pm 7.85	84.84 \pm 2.29	85.27 \pm 1.57	82.15 \pm 2.24	83.74 \pm 1.11	76.24 \pm 2.98	68.60 \pm 7.28	84.23 \pm 1.49	79.20 \pm 1.80	79.69 \pm 1.19	83.94 \pm 0.95	87.49 \pm 1.26	87.63 \pm 0.58
	Average	72.72	80.80	83.62	83.51	82.18	75.46	69.30	83.49	77.44	81.76	81.05	84.48	86.70

Table 3: Accuracy score (% \pm standard deviation) of node classification task on real-world datasets against non-targeted attack.

Dataset	Attack	GCN	GSR	GARNET	GUARD	SVD	Jaccard	RGCN	MedianGCN	GNNGuard	SoftMedian	ElasticGCN	GraphAT	DiffSP
Cora	MinMax	59.91 \pm 2.60	67.80 \pm 2.18	65.68 \pm 0.58	61.62 \pm 2.85	64.75 \pm 0.96	64.43 \pm 2.48	62.49 \pm 2.19	56.35 \pm 3.34	63.63 \pm 2.40	74.53 \pm 0.70	17.05 \pm 5.33	63.35 \pm 2.60	75.00 \pm 1.12
	DICE	69.58 \pm 2.17	74.55 \pm 0.74	68.88 \pm 1.08	71.50 \pm 2.68	59.52 \pm 0.39	71.89 \pm 0.56	69.92 \pm 0.97	71.61 \pm 0.72	68.82 \pm 0.95	73.38 \pm 0.68	74.11 \pm 1.28	75.84 \pm 0.57	75.96 \pm 0.87
	Random	70.43 \pm 2.22	77.37 \pm 0.88	75.63 \pm 0.93	74.96 \pm 0.51	62.54 \pm 0.65	73.74 \pm 0.60	72.74 \pm 1.00	74.31 \pm 0.95	68.33 \pm 1.72	77.52 \pm 0.65	74.06 \pm 3.87	77.39 \pm 0.91	77.63 \pm 0.80
	Average	66.64	73.24	70.06	69.36	62.27	70.02	68.38	67.42	66.93	75.14	55.07	72.19	76.20
CiteSeer	MinMax	52.07 \pm 6.63	54.74 \pm 4.92	59.00 \pm 2.35	58.02 \pm 1.44	35.83 \pm 1.89	56.65 \pm 3.81	42.85 \pm 7.72	53.39 \pm 3.44	57.98 \pm 2.97	60.84 \pm 1.40	17.05 \pm 5.33	61.54 \pm 3.70	61.59 \pm 1.10
	DICE	57.46 \pm 1.63	62.48 \pm 1.08	55.59 \pm 3.01	62.19 \pm 0.99	57.33 \pm 0.49	63.00 \pm 0.87	50.88 \pm 1.59	59.95 \pm 0.97	58.85 \pm 3.22	59.85 \pm 0.81	60.30 \pm 1.46	65.28 \pm 0.81	65.43 \pm 0.70
	Random	56.19 \pm 3.08	64.01 \pm 1.08	56.34 \pm 3.70	62.47 \pm 0.88	54.54 \pm 0.62	64.20 \pm 0.46	50.13 \pm 1.95	60.60 \pm 0.81	61.51 \pm 3.32	58.66 \pm 1.49	58.00 \pm 3.61	64.94 \pm 1.12	66.78 \pm 0.54
	Average	52.24	60.41	56.98	60.89	49.23	61.28	47.95	57.98	59.45	59.78	45.12	63.92	64.60
PolBlogs	MinMax	86.96 \pm 0.43	88.56 \pm 0.82	87.85 \pm 0.19	89.51 \pm 0.85	87.11 \pm 0.32	51.01 \pm 1.75	87.04 \pm 0.19	87.95 \pm 4.81	50.32 \pm 1.19	88.76 \pm 0.37	87.33 \pm 0.62	88.32 \pm 0.35	89.52 \pm 3.08
	DICE	76.52 \pm 2.76	80.75 \pm 4.72	85.05 \pm 1.01	83.76 \pm 0.78	82.84 \pm 0.20	50.27 \pm 1.91	81.50 \pm 0.44	74.19 \pm 3.02	50.79 \pm 1.59	86.47 \pm 0.45	82.40 \pm 2.24	87.39 \pm 0.44	88.85 \pm 1.32
	Random	83.24 \pm 5.81	87.81 \pm 1.03	83.42 \pm 1.59	87.48 \pm 1.51	85.59 \pm 0.31	51.02 \pm 1.75	85.46 \pm 0.40	83.57 \pm 2.71	50.28 \pm 1.13	90.35 \pm 0.56	49.50 \pm 2.20	90.50 \pm 0.56	92.61 \pm 0.93
	Average	82.24	85.71	85.44	86.92	85.18	50.77	84.67	81.90	50.46	88.53	73.08	88.74	90.33
Photo	MinMax	73.12 \pm 3.17	76.36 \pm 3.09	81.75 \pm 1.91	75.89 \pm 3.28	69.92 \pm 5.50	74.20 \pm 3.94	87.04 \pm 0.19	67.43 \pm 4.31	71.44 \pm 6.66	85.23 \pm 2.12	8.56 \pm 3.24	81.70 \pm 2.48	88.51 \pm 0.61
	DICE	84.60 \pm 1.17	82.52 \pm 1.66	85.43 \pm 0.92	82.92 \pm 1.27	76.42 \pm 1.39	83.20 \pm 1.44	81.57 \pm 0.44	82.83 \pm 2.45	83.87 \pm 1.19	84.72 \pm 0.90	81.86 \pm 3.61	87.22 \pm 1.13	83.52 \pm 1.19
	Random	85.38 \pm 1.76	83.62 \pm 2.91	84.12 \pm 3.95	85.49 \pm 1.55	79.13 \pm 2.84	83.37 \pm 1.93	86.87 \pm 2.89	84.07 \pm 2.52	83.24 \pm 4.83	85.95 \pm 1.06	75.32 \pm 2.38	86.23 \pm 2.26	84.60 \pm 0.46
	Average	81.03	80.83	83.77	81.43	75.16	80.26	85.16	78.11	79.52	85.30	55.25	85.05	85.54

We evaluate variants on the IMDB-BINARY and COLLAB datasets under PR-BCD and GradArgmax attacks for graph classification and on the Cora and CiteSeer dataset under PR-BCD and MinMax attacks for node classification. Results are shown in Figure 3.

Result. DiffSP consistently outperforms the other variants. DiffSP (w/o LN) over-perturbs the valuable parts of the graph leading to degraded performance. Similarly, DiffSP (w/o TG) increases the uncertainty of generation, causing deviations from the target clean graph. These reduce the robustness against evasion attacks.

5.3 Study on Cross-Dataset Generalization

We assess DiffSP’s generalization ability. The goal is to determine whether DiffSP effectively learns the predictive patterns of clean graphs. We train DiffSP on IMDB-BINARY and use the trained model to purify graphs on IMDB-MULTI, and vice versa.

Result. As shown in Table 4, DiffSP trained on different datasets, still demonstrates strong robustness compared to GCN trained and tested on the same dataset. Furthermore, DiffSP exhibits only a small performance gap compared to when it is trained and tested on the same dataset directly. These results highlight DiffSP’s ability to learn the underlying clean distribution of a category of data and capture predictive patterns that generalize across diverse datasets.

Table 4: Accuracy (% \pm standard deviation) across datasets. (B \rightarrow B) indicates the model is both trained and tested on IMDB-BINARY, while (M \rightarrow B) indicates the model is trained on IMDB-MULTI but tested on IMDB-BINARY.

Attack	GCN (B \rightarrow B)	DiffSP (B \rightarrow B)	DiffSP (M \rightarrow B)	GCN (B \rightarrow B)	DiffSP (M \rightarrow M)	DiffSP (B \rightarrow M)
PR-BCD	50.90 \pm 1.92	74.10 \pm 1.29	73.90 \pm 2.02	35.00 \pm 1.31	47.00 \pm 1.44	45.33 \pm 0.99
GradArgmax	62.80 \pm 1.08	76.00 \pm 1.15	75.00 \pm 1.70	38.53 \pm 2.00	48.47 \pm 1.12	47.60 \pm 1.41
CAMA	52.20 \pm 1.33	75.90 \pm 0.99	75.10 \pm 1.37	38.40 \pm 1.69	48.13 \pm 2.44	47.47 \pm 0.88

5.4 Study on Purification Steps

We evaluate the performance as the number of diffusion steps varies. For graph classification on the IMDB-BINARY dataset, we adjust the diffusion steps from 1 to 9 under GradArgMax, PR-BCD, and CAMA-Subgraph attacks. For node classification on the Cora dataset, we vary the diffusion steps from 1 to 12 under the GR-BCD, PR-BCD, and MinMax attacks. The results are shown in Figure 4.

Result. We observe that all-time step settings demonstrate the ability to effectively purify adversarial graphs. At smaller time steps, the overall trend shows increasing accuracy as the number of diffusion steps increases. This is likely because fewer time steps do not introduce enough noise to sufficiently suppress the adversarial

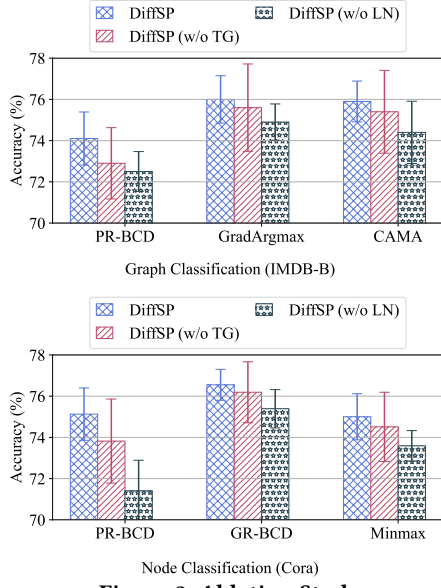


Figure 3: Ablation Study

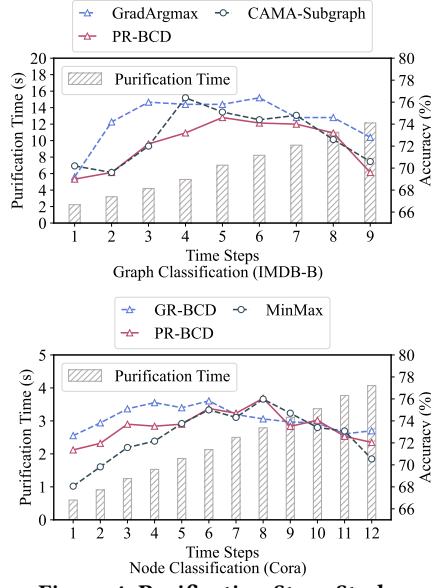


Figure 4: Purification Steps Study

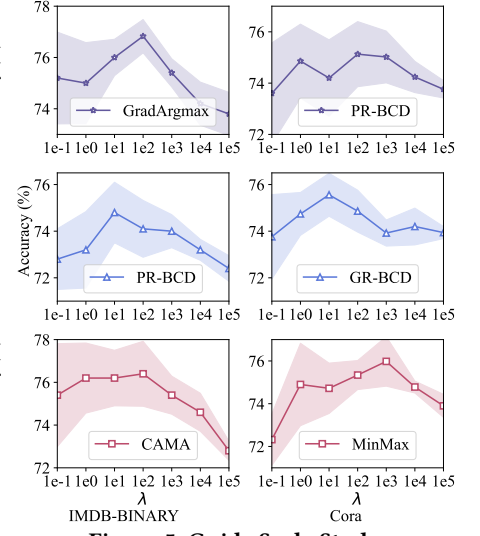


Figure 5: Guide Scale Study

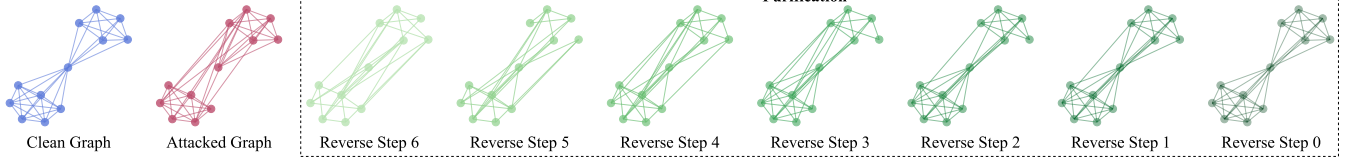


Figure 6: Visualization Study

information in the graph. As the diffusion steps increase, we do not see a significant decline in performance. This stability can be attributed to our LID-Driven Non-Isotropic Diffusion Mechanism, which minimizes over-perturbation of the clean graph parts. Additionally, we found that the time required for purifying increased linearly.

5.5 Study on Scale of Graph Transfer Entropy

To analyze the impact of the guidance scale λ , we vary λ from $1e^{-1}$ to $1e^5$. The results are presented in Figure 5. For graph classification, experiments are conducted on the IMDB-BINARY dataset under the GradArgmax, PR-BCD, and CAMA-Subgraph attacks. For node classification, experiments are performed on the Cora dataset under the PR-BCD, GR-BCD, and MinMax attacks.

Result. The results show that smaller values of λ have minimal effect on accuracy. However, they reduce the stability of the purification during the reverse denoising process, leading to a higher standard deviation. This instability arises because the model is less effective at reducing uncertainty and guiding the generation process when λ is too small. On the other hand, large λ values decrease accuracy by overemphasizing guidance, causing the model to reintroduce adversarial information into the generated graph.

5.6 Graph Purification Visualization

We visualize snapshots of different purification time steps on the IMDB-BINARY dataset using NetworkX [19], as shown in Figure 6. The visualization process demonstrates that DiffSP has mastered the ability to generate clean graphs, achieving graph purification.

6 Conclusion

Under evasion attacks, most existing methods rely on priors to enhance robustness, which limits their effectiveness. To address this, we propose a novel framework named DiffSP, which achieves prior-free structure purification across diverse evasion attacks and datasets. DiffSP innovatively adopts the graph diffusion model to learn the clean graph distribution and purify the attacked graph under the direction of captured predictive patterns. To precisely denoise the attacked graph without disrupting the clean structure, we design an LID-Driven Non-Isotropic Diffusion Mechanism to inject varying levels of noise into each node based on their adversarial degree. To align the semantic information between the generated graph and the target clean graph, we design a Graph Transfer Entropy Guided Denoising Mechanism to reduce generation uncertainty and guide the generation direction. Extensive experimental results demonstrate that DiffSP enhances the robustness of graph learning in various scenarios. In future work, we aim to incorporate feature-based attack experiments and optimize the time complexity of DiffSP. Additionally, we plan to improve our proposed graph entropy tool and explore its application. Details about the limitations and future directions can be found in Appendix E.

Acknowledgments

The corresponding author is Qingyun Sun. The authors of this paper are supported by the National Natural Science Foundation of China through grants No.62225202, and No.62302023. We owe sincere thanks to all authors for their valuable efforts and contributions.

References

- [1] Lada A Adamic and Natalie Glance. 2005. The political blogosphere and the 2004 US election: divided they blog. In *LinkKDD*. 36–43.
- [2] Laurent Amsaleg, Oussama Chelly, Teddy Furon, Stéphane Girard, Michael E Houle, Ken-ichi Kawarabayashi, and Michael Nett. 2015. Estimating local intrinsic dimensionality. In *KDD*. 29–38.
- [3] Jacob Austin, Daniel D Johnson, Jonathan Ho, Daniel Tarlow, and Rianne Van Den Berg. 2021. Structured denoising diffusion models in discrete state-spaces. *NeurIPS* 34 (2021), 17981–17993.
- [4] Sambaran Bandyopadhyay, Manasvi Aggarwal, and M Narasimha Murty. 2020. Hierarchically Attentive Graph Pooling with Subgraph Attention. In *ICML*.
- [5] Battista Biggio, Igino Corona, Davide Maiorca, Blaine Nelson, Nedim Šrđić, Pavel Laskov, Giorgio Giacinto, and Fabio Roli. 2013. Evasion attacks against machine learning at test time. In *ECML*. Springer, Springer, 387–402.
- [6] Liang Chen, Jintang Li, Qibiao Peng, Yang Liu, Zibin Zheng, and Carl Yang. 2021. Understanding structural vulnerability in graph convolutional networks. In *IJCAI*.
- [7] Tianyi Chen and Charalampos Tsourakakis. 2022. Antibenford subgraphs: Unsupervised anomaly detection in financial networks. In *KDD*. 2762–2770.
- [8] Xiaohui Chen, Jiaying He, Xu Han, and Li-Ping Liu. 2023. Efficient and degree-guided graph generation via discrete diffusion modeling. In *ICML*. 4585–4610.
- [9] Yu Chen, Lingfei Wu, and Mohammed Zaki. 2020. Iterative deep graph learning for graph neural networks: Better and robust node embeddings. *NeurIPS* 33 (2020), 19314–19326.
- [10] Hanjun Dai, Hui Li, Tian Tian, Xin Huang, Lin Wang, Jun Zhu, and Le Song. 2018. Adversarial attack on graph structured data. In *ICML*. PMLR, 1115–1124.
- [11] Chenhui Deng, Xiuyu Li, Zhuo Feng, and Zhiru Zhang. 2022. Garnet: Reduced-rank topology learning for robust and scalable graph neural networks. In *LoG*. PMLR, 3–1.
- [12] Ivan Dokmanic, Reza Parhizkar, Juri Ranieri, and Martin Vetterli. 2015. Euclidean distance matrices: essential theory, algorithms, and applications. *IEEE Signal Processing Magazine* 32, 6 (2015), 12–30.
- [13] Negin Entezari, Saba A Al-Sayouri, Amirali Darvishzadeh, and Evangelos E Papalexakis. 2020. All you need is low (rank) defending against adversarial attacks on graphs. In *WSDM*. 169–177.
- [14] Reuben Feinman, Ryan R Curtin, Saurabh Shintre, and Andrew B Gardner. 2017. Detecting adversarial samples from artifacts. *arXiv preprint arXiv:1703.00410* (2017).
- [15] Xingcheng Fu, Yisen Gao, Yuecen Wei, Qingyun Sun, Hao Peng, Jianxin Li, and Xianxian Li. 2024. Hyperbolic Geometric Latent Diffusion Model for Graph Generation. In *ICML*.
- [16] Yarín Gal and Zoubin Ghahramani. 2016. Dropout as a bayesian approximation: Representing model uncertainty in deep learning. In *ICML*. PMLR, 1050–1059.
- [17] Simon Geisler, Tobias Schmidt, Hakan Şirin, Daniel Zügner, Aleksandar Bojchevski, and Stephan Günnemann. 2021. Robustness of graph neural networks at scale. *NeurIPS* 34 (2021), 7637–7649.
- [18] Kilian Konstantin Haefeli, Karolis Martinkus, Nathanaël Perraudin, and Roger Wattenhofer. 2022. Diffusion models for graphs benefit from discrete state spaces. In *NeurIPS*.
- [19] Aric Hagberg, Pieter Swart, and Daniel S Chult. 2008. *Exploring network structure, dynamics, and function using NetworkX*. Technical Report. Los Alamos National Lab.(LANL), Los Alamos, NM (United States).
- [20] Xiaotian Han, Zhimeng Jiang, Ninghao Liu, and Xia Hu. 2022. G-mixup: Graph data augmentation for graph classification. In *ICML*. PMLR, 8230–8248.
- [21] Michael E Houle. 2017. Local intrinsic dimensionality I: an extreme-value-theoretic foundation for similarity applications. In *SISAP*. Springer, 64–79.
- [22] Yeonjun In, Kanghoon Yoon, Kibum Kim, Kijung Shin, and Chanyoung Park. 2024. Self-Guided Robust Graph Structure Refinement. In *WWW*. 697–708.
- [23] Yeonjun In, Kanghoon Yoon, and Chanyoung Park. 2023. Similarity preserving adversarial graph contrastive learning. In *KDD*. 867–878.
- [24] Sergei Ivanov, Sergei Sviridov, and Evgeny Burnaev. 2019. Understanding isomorphism bias in graph data sets. *arXiv preprint arXiv:1910.12091* (2019).
- [25] Wei Jin, Tyler Derr, Yiqi Wang, Yao Ma, Zitao Liu, and Jiliang Tang. 2021. Node similarity preserving graph convolutional networks. In *WWW*. 148–156.
- [26] Wei Jin, Yao Ma, Xiaorui Liu, Xianfeng Tang, Suhang Wang, and Jiliang Tang. 2020. Graph structure learning for robust graph neural networks. In *KDD*. 66–74.
- [27] Jaehyeong Jo, Seul Lee, and Sung Ju Hwang. 2022. Score-based generative modeling of graphs via the system of stochastic differential equations. In *ICML*. PMLR, 10362–10383.
- [28] Thomas N Kipf and Max Welling. 2016. Semi-supervised classification with graph convolutional networks. In *ICLR*.
- [29] Jintang Li, Jie Liao, Ruofan Wu, Liang Chen, Zibin Zheng, Jiawang Dan, Changhua Meng, and Weiqiang Wang. 2023. GUARD: Graph universal adversarial defense. In *CIKM*. 1198–1207.
- [30] Kuan Li, Yang Liu, Xiang Ao, and Qing He. 2023. Revisiting graph adversarial attack and defense from a data distribution perspective. In *ICLR*.
- [31] Mufei Li, Eleonora Kreačić, Vamsi K Potluru, and Pan Li. 2023. Graphmaker: Can diffusion models generate large attributed graphs? *arXiv* (2023).
- [32] Yaxin Li, Wei Jin, Han Xu, and Jiliang Tang. 2020. Deeprobust: A pytorch library for adversarial attacks and defenses. *arXiv* (2020).
- [33] Yujia Li, Oriol Vinyals, Chris Dyer, Razvan Pascanu, and Peter Battaglia. 2018. Learning deep generative models of graphs. *ICLR* (2018).
- [34] Xiaorui Liu, Wei Jin, Yao Ma, Yaxin Li, Hua Liu, Yiqi Wang, Ming Yan, and Jiliang Tang. 2021. Elastic graph neural networks. In *ICML*. PMLR, 6837–6849.
- [35] Gui-Fu Lu, Yong Wang, and Ganyi Tang. 2022. Robust low-rank representation with adaptive graph regularization from clean data. *Applied Intelligence* 52, 5 (2022), 5830–5840.
- [36] Guanghui Ma, Chunming Hu, Ling Ge, and Hong Zhang. 2023. Multi-View Robust Graph Representation Learning for Graph Classification.. In *IJCAI*. 4037–4045.
- [37] Xingjun Ma, Bo Li, Yisen Wang, Sarah M Erfani, Sudanthi Wijewickrema, Grant Schoenebeck, Dawn Song, Michael E Houle, and James Bailey. 2018. Characterizing adversarial subspaces using local intrinsic dimensionality. In *ICLR*.
- [38] Alexander Quinn Nichol and Prafulla Dhariwal. 2021. Improved denoising diffusion probabilistic models. In *ICML*. PMLR, 8162–8171.
- [39] Chenhao Niu, Yang Song, Jiaming Song, Shengjia Zhao, Aditya Grover, and Stefano Ermon. 2020. Permutation invariant graph generation via score-based generative modeling. In *AISTATS*. PMLR, 4474–4484.
- [40] Thomas Schreiber. 2000. Measuring information transfer. *Physical review letters* 85, 2 (2000), 461.
- [41] Aleksandr Shchur, Maximilian Mumme, Aleksandar Bojchevski, and Stephan Günnemann. 2018. Pitfalls of graph neural network evaluation. *arXiv* (2018).
- [42] Yunsheng Shi, Zhengjie Huang, Shikun Feng, Hui Zhong, Wenjin Wang, and Yu Sun. 2020. Masked label prediction: Unified message passing model for semi-supervised classification. In *IJCAI*.
- [43] Bernard W Silverman. 2018. *Density estimation for statistics and data analysis*. Routledge.
- [44] Jascha Sohl-Dickstein, Eric Weiss, Niru Maheswaranathan, and Surya Ganguli. 2015. Deep unsupervised learning using nonequilibrium thermodynamics. In *ICML*. PMLR, 2256–2265.
- [45] Yang Song and Stefano Ermon. 2019. Generative modeling by estimating gradients of the data distribution. *NeurIPS* 32 (2019).
- [46] Lichao Sun, Yingtong Dou, Carl Yang, Kai Zhang, Ji Wang, S Yu Philip, Lifang He, and Bo Li. 2022. Adversarial attack and defense on graph data: A survey. *TKDE* 35, 8 (2022), 7693–7711.
- [47] Qingyun Sun, Jianxin Li, Hao Peng, Jia Wu, Xingcheng Fu, Cheng Ji, and S Yu Philip. 2022. Graph structure learning with variational information bottleneck. In *AAAI*, Vol. 36. 4165–4174.
- [48] Xianfeng Tang, Yandong Li, Yiwei Sun, Huaxiu Yao, Prasenjit Mitra, and Suhang Wang. 2020. Transferring robustness for graph neural network against poisoning attacks. In *WWW*. 600–608.
- [49] Clement Vignac, Igor Krawczuk, Antoine Siraudin, Bohan Wang, Volkan Cevher, and Pascal Frossard. 2022. Digress: Discrete denoising diffusion for graph generation. In *ICLR*.
- [50] Vikram Voleti, Christopher Pal, and Adam Oberman. 2022. Score-based denoising diffusion with non-isotropic gaussian noise models. *arXiv preprint arXiv:2210.12254* (2022).
- [51] Xin Wang, Heng Chang, Beini Xie, Tian Bian, Shiji Zhou, Daixin Wang, Zhiqiang Zhang, and Wenwu Zhu. 2023. Revisiting adversarial attacks on graph neural networks for graph classification. *TKDE* (2023).
- [52] Huijun Wu, Chen Wang, Yuriy Tyshetskiy, Andrew Docherty, Kai Lu, and Liming Zhu. 2019. Adversarial examples on graph data: Deep insights into attack and defense. In *IJCAI*.
- [53] Junran Wu, Xueyuan Chen, Ke Xu, and Shangzhe Li. 2022. Structural entropy guided graph hierarchical pooling. In *ICML*. PMLR, 24017–24030.
- [54] Shiwen Wu, Fei Sun, Wentao Zhang, Xu Xie, and Bin Cui. 2022. Graph neural networks in recommender systems: a survey. *Comput. Surveys* 55, 5 (2022), 1–37.
- [55] Ying-Xin Wu, Xiang Wang, An Zhang, Xiangnan He, and Tat-Seng Chua. 2022. Discovering invariant rationales for graph neural networks. In *ICLR*.
- [56] Aaron D Wyner. 1978. A definition of conditional mutual information for arbitrary ensembles. *Information and Control* 38, 1 (1978), 51–59.
- [57] Hui Xu, Liyao Xiang, Jiahao Yu, Anqi Cao, and Xinbing Wang. 2021. Speedup robust graph structure learning with low-rank information. In *CIKM*. 2241–2250.
- [58] Kaidi Xu, Hongge Chen, Sijia Liu, Pin-Yu Chen, Tsui Wei Weng, Mingyi Hong, and Xue Lin. 2019. Topology attack and defense for graph neural networks: An optimization perspective. In *IJCAI*.
- [59] Zhilin Yang, William Cohen, and Ruslan Salakhudinov. 2016. Revisiting semi-supervised learning with graph embeddings. In *ICML*. PMLR, 40–48.
- [60] Yuning You, Tianlong Chen, Yongduo Sui, Ting Chen, Zhangyang Wang, and Yang Shen. 2020. Graph contrastive learning with augmentations. *NeurIPS* 33 (2020), 5812–5823.
- [61] Junchi Yu, Jie Cao, and Ran He. 2022. Improving subgraph recognition with variational graph information bottleneck. In *CVPR*. 19396–19405.

- [62] Shujian Yu, Luis Gonzalo Sanchez Giraldo, Robert Jenssen, and Jose C Principe. 2019. Multivariate Extension of Matrix-Based Rényi's α -Order Entropy Functional. *TPAMI* 42, 11 (2019), 2960–2966.
- [63] Xi Yu, Xiang Gu, Haozhi Liu, and Jian Sun. 2024. Constructing non-isotropic Gaussian diffusion model using isotropic Gaussian diffusion model for image editing. *NeurIPS* 36 (2024).
- [64] Xiang Zhang and Marinka Zitnik. 2020. GnnGuard: Defending graph neural networks against adversarial attacks. *NeurIPS* 33 (2020), 9263–9275.
- [65] Zhen Zhang, Jiajun Bu, Martin Ester, Jianfeng Zhang, Chengwei Yao, Zhi Yu, and Can Wang. 2019. Hierarchical graph pooling with structure learning. *arXiv* (2019).
- [66] Zhongjian Zhang, Xiao Wang, Huichi Zhou, Yue Yu, Mengmei Zhang, Cheng Yang, and Chuan Shi. 2024. Can Large Language Models Improve the Adversarial Robustness of Graph Neural Networks? *arXiv* (2024).
- [67] Jianan Zhao, Qianlong Wen, Mingxuan Ju, Chuxu Zhang, and Yanfang Ye. 2023. Self-supervised graph structure refinement for graph neural networks. In *WSDM*. 159–167.
- [68] Zhe Zhao, Pengkun Wang, Haibin Wen, Yudong Zhang, Binwu Wang, and Yang Wang. 2024. Graph Networks Stand Strong: Enhancing Robustness via Stability Constraints. In *ICASSP*. IEEE, 7315–7319.
- [69] Zhilun Zhou, Yu Liu, Jingtao Ding, Depeng Jin, and Yong Li. 2023. Hierarchical knowledge graph learning enabled socioeconomic indicator prediction in location-based social network. In *WWW*. 122–132.
- [70] Dingyuan Zhu, Ziwei Zhang, Peng Cui, and Wenwu Zhu. 2019. Robust graph convolutional networks against adversarial attacks. In *KDD*. 1399–1407.
- [71] Daniel Zügner, Amir Akbarnejad, and Stephan Günnemann. 2018. Adversarial attacks on neural networks for graph data. In *KDD*. 2847–2856.
- [72] Daniel Zügner and Stephan Günnemann. 2019. Adversarial Attacks on Graph Neural Networks via Meta Learning. In *ICLR*.

A Proof and Derivation

A.1 Proof of Proposition 1

We first restate Proposition 1.

PROPOSITION 1. *For each edge at time t , the adjacency matrix is updated as $\mathbf{A}_{ij}^{(t)} = \mathbf{A}_{ij}(\tilde{\mathbf{Q}}_A^{(t)})_{ij}$, where the non-isotropic transition matrix is $(\tilde{\mathbf{Q}}_A^{(t)})_{ij} = \bar{\alpha}^{(t)}\mathbf{I} + (\Lambda_{\mathbf{A}})_{ij}(1 - \bar{\alpha})\mathbf{1}\mathbf{m}_A^T$. There exists a unique time $\hat{t}(\mathbf{A}_{ij}) \in [0, T]$ such that $(\tilde{\mathbf{Q}}_A^{(t)})_{ij} \Leftrightarrow (\tilde{\mathbf{Q}}_A^{\hat{t}(\mathbf{A}_{ij})})_{ij}$, where:*

$$\hat{t}(\mathbf{A}_{ij}) = T \left(\frac{2(1+s)}{\pi} \cos^{-1} \left(\sqrt{\frac{\bar{\alpha}^{(t)}}{[\Lambda(\mathbf{A})_{ij}(1 - \bar{\alpha}^{(t)}) + \bar{\alpha}^{(t)}]}} \right) - s \right).$$

PROOF. $\tilde{\mathbf{Q}}_A^{(t)} = \bar{\alpha}^{(t)}\mathbf{I} + (1 - \bar{\alpha}^{(t)})\mathbf{1}\mathbf{m}_A^T$ indicates the degree of noise added to the adjacency matrix \mathbf{A} at time step t . Let $\text{SNR}_{\tilde{\mathbf{Q}}_A^{(t)}}(t)$ denotes the signal-to-noise of $\tilde{\mathbf{Q}}_A^{(t)}$ at time step t , we have:

$$\text{SNR}_{\tilde{\mathbf{Q}}_A^{(t)}}(t) = \frac{1 - \bar{\alpha}^{(t)}}{\bar{\alpha}^{(t)}}. \quad (\text{A.1})$$

Such that:

$$(\tilde{\mathbf{Q}}_A^{(t)})_{ij} \Leftrightarrow (\tilde{\mathbf{Q}}_A^{\hat{t}(\mathbf{A}_{ij})})_{ij} \quad (\text{A.2})$$

$$\Rightarrow \text{SNR}_{\tilde{\mathbf{Q}}_A^{(t)}}(t) = \text{SNR}_{\tilde{\mathbf{Q}}_A^{\hat{t}(\mathbf{A}_{ij})}}(\hat{t}(\mathbf{A}_{ij})) \quad (\text{A.3})$$

$$\Rightarrow \frac{(\Lambda_{\mathbf{A}})_{ij}(1 - \bar{\alpha}^{(t)})}{\bar{\alpha}^{(t)}} = \frac{1 - \bar{\alpha}^{(\hat{t}(\mathbf{A}_{ij}))}}{\bar{\alpha}^{(\hat{t}(\mathbf{A}_{ij}))}}. \quad (\text{A.4})$$

We first prove that for each time step t , there exists and only exists one t' that satisfies $(\tilde{\mathbf{Q}}_A^{(t)})_{ij} \Leftrightarrow (\tilde{\mathbf{Q}}_A^{\hat{t}(\mathbf{A}_{ij})})_{ij}$. Left $g(t') = \frac{(\Lambda_{\mathbf{A}})_{ij}(1 - \bar{\alpha}^{(t)})}{\bar{\alpha}^{(t)}} - \frac{1 - \bar{\alpha}^{(t')}}{\bar{\alpha}^{(t'')}}$ represents the function of $t' \in [0, T]$. $\bar{\alpha}^{(t)} = \cos^2 \left(\frac{t/T+s}{1+s} \cdot \frac{\pi}{2} \right)$ is the scheduler with a small constant s . We have $\alpha^{(0)} = \cos^2 \left(\frac{0+s}{1+s} \cdot \frac{\pi}{2} \right) \approx \cos^2(0) = 0$, and $\alpha^{(T)} = \cos^2 \left(\frac{1+s}{1+s} \cdot \frac{\pi}{2} \right) = \cos^2 \left(\frac{\pi}{2} \right) = 1$. It is known that $(1 - \bar{\alpha})$ monotonically decreasing over the domain, while $\bar{\alpha}$ monotonically increasing, with $1 - \bar{\alpha} > 0$ and

$\bar{\alpha} > 0$. Therefore, $g(t')$ is a monotonic function over the domain. So we achieve:

$$g(0) = \frac{(\Lambda_{\mathbf{A}})_{ij}(1 - \bar{\alpha}^{(t)})}{\bar{\alpha}^{(t)}} - 0 > 0. \quad (\text{A.5})$$

Having $\Lambda(\mathbf{A})_{ij} \in [0, 1]$ indicates the node adversarial score, we can then derive the following:

$$g(T) = \frac{(\Lambda_{\mathbf{A}})_{ij}(1 - \bar{\alpha}^{(t)})}{\bar{\alpha}^{(t)}} - 1 \quad (\text{A.6})$$

$$< \frac{(1 - \bar{\alpha}^{(t)})}{\bar{\alpha}^{(t)}} - 1 \quad (\text{A.7})$$

$$< 0. \quad (\text{A.8})$$

Thus, we have $g(0)g(T) < 0$, and since $g(t')$ is a monotonically decreasing function, the intermediate value theorem guarantees that there exists exactly one $t'_0 \in [0, T]$ satisfies $g(t'_0) = 0$. By setting $g(t') = 0$, we obtain:

$$\Lambda(\mathbf{A})_{ij}\bar{\alpha}^{(t')}(1 - \bar{\alpha}^{(t')}) = \bar{\alpha}^{(t')}(1 - \bar{\alpha}^{(t')}) \quad (\text{A.9})$$

$$\Rightarrow \bar{\alpha}^{(t')} [\Lambda(\mathbf{A})_{ij}(1 - \bar{\alpha}^{(t')}) + \bar{\alpha}^{(t')}] = \bar{\alpha}^{(t')} \quad (\text{A.10})$$

$$\Rightarrow \bar{\alpha}^{(t')} = \frac{\bar{\alpha}^{(t')}}{[\Lambda(\mathbf{A})_{ij}(1 - \bar{\alpha}^{(t')}) + \bar{\alpha}^{(t')}] } \quad (\text{A.11})$$

$$\Rightarrow t' = T \left(\frac{2(1+s)}{\pi} \cos^{-1} \left(\sqrt{\frac{\bar{\alpha}^{(t)}}{[\Lambda(\mathbf{A})_{ij}(1 - \bar{\alpha}^{(t)}) + \bar{\alpha}^{(t)}]}} \right) - s \right). \quad (\text{A.12})$$

This concludes the proof of the proposition. \square

A.2 Graph Transfer Entropy Derivation

We first restate Eq. (7).

$$I(\hat{G}^{t-1}; G_{\text{adv}} | \hat{G}_t) = H(\hat{G}^{(t-1)} | \hat{G}_t) - H(\hat{G}^{(t-1)} | \hat{G}_t, G_{\text{adv}}).$$

According to the definition of mutual information:

$$I(\hat{G}^{t-1}; G_{\text{adv}} | \hat{G}_t) \quad (\text{A.13})$$

$$= H(\hat{G}^{(t-1)} | \hat{G}_t) - H(\hat{G}^{(t-1)} | \hat{G}_t, G_{\text{adv}}) \quad (\text{A.14})$$

$$= \frac{H(\hat{G}^{(t-1)}, \hat{G}_t)}{H(\hat{G}_t)} - \frac{H(\hat{G}^{(t-1)}, \hat{G}_t, G_{\text{adv}})}{H(\hat{G}_t, G_{\text{adv}})}. \quad (\text{A.15})$$

Then combined with Eq. (9), we have:

$$I(\hat{G}^{t-1}; G_{\text{adv}} | \hat{G}_t) \quad (\text{A.16})$$

$$= S_{\alpha} \left(\frac{\hat{\mathbf{K}}^{(t-1)} \odot \hat{\mathbf{K}}^{(t)}}{\text{tr}(\hat{\mathbf{K}}^{(t-1)} \odot \hat{\mathbf{K}}^{(t)})} \right) / S_{\alpha}(\hat{\mathbf{K}}^{(t)}) \quad (\text{A.17})$$

$$- S_{\alpha} \left(\frac{\hat{\mathbf{K}}^{(t-1)} \odot \hat{\mathbf{K}}^{(t)} \odot \mathbf{K}_{\text{adv}}}{\text{tr}(\hat{\mathbf{K}}^{(t-1)} \odot \hat{\mathbf{K}}^{(t)} \odot \mathbf{K}_{\text{adv}})} \right) / S_{\alpha} \left(\frac{\hat{\mathbf{K}}^{(t)} \odot \mathbf{K}_{\text{adv}}}{\text{tr}(\hat{\mathbf{K}}^{(t)} \odot \mathbf{K}_{\text{adv}})} \right), \quad (\text{A.18})$$

where $S_{\alpha}(\cdot)$ is the graph entropy calculated according to Eq. (8) and $\hat{\mathbf{K}}^{(t-1)}$, $\hat{\mathbf{K}}^{(t)}$, \mathbf{K}_{adv} is the Gram matrix of $\hat{\mathbf{A}}^{(t-1)}$, $\hat{\mathbf{A}}^{(t)}$, \mathbf{A}_{adv} .

B Detailed Understanding of the Proposed Graph Transfer Entropy

In this subsection, we further elaborate on the understanding of our graph entropy estimation method in Eq. (8). After message passing, the set of node representations \mathbf{Z} can be treated as variables that

capture both structural and node feature neighborhood information. The normalized Gram matrix $\hat{\mathbf{K}}$, obtained by applying a positive definite kernel on all pairs of z , measures the neighborhood similarity between each pair of nodes, taking into account both node features and neighboring structures. Let $\lambda_i(\hat{\mathbf{K}})$ be the eigenvalue of $\hat{\mathbf{K}}$ with eigenvector \mathbf{x}_i . Then we have:

$$\hat{\mathbf{K}}^2 = \hat{\mathbf{K}}(\hat{\mathbf{K}}\mathbf{x}_i) = \hat{\mathbf{K}}(\lambda_i(\hat{\mathbf{K}})\mathbf{x}_i) = \lambda_i(\hat{\mathbf{K}})\hat{\mathbf{K}}\mathbf{x}_i = \lambda_i^2(\hat{\mathbf{K}})\mathbf{x}_i. \quad (\text{B.19})$$

Thus we achieve:

$$\sum_{i=1}^n \lambda_i^\alpha(\hat{\mathbf{K}}) = \sum_{i=1}^n \lambda_i(\hat{\mathbf{K}}^\alpha). \quad (\text{B.20})$$

Since the sum of all eigenvalues of a matrix is the trace of the matrix, the graph entropy is determined by the trace of $\hat{\mathbf{K}}^\alpha$. By setting $\alpha = 2$, $\hat{\mathbf{K}}_{ii}^2$ describes the similarity of node i with all other nodes, considering both node features and neighboring structures. When $\alpha = 2$, the graph entropy can be expressed as: $H(G) = -\log \text{tr}(\hat{\mathbf{K}}^2)$. Therefore a lower graph entropy indicates a graph with a stronger community structure, while a higher graph entropy suggests a more chaotic graph structure with less regularity. So maximizing the transfer entropy $I(\hat{G}^{(t-1)}; G_{\text{adv}} | \hat{G}^{(t)})$ actually encourage the community structure of $\hat{G}^{(t-1)}$ move towards G_{adv} .

C Computational Complexity Analysis

The overall time complexity is $O(N^2)$, where N represents the number of nodes. Specifically, the graph diffusion purification model has a complexity of $O(TN^2)$. The LID-Driven Non-Isotropic Diffusion Module has a complexity of $O(N)$, and the Transfer Entropy Guided Diffusion Module has a complexity of $O(N^2)$. Therefore, the overall time complexity of the purification process is $O(TN^2) + O(N) + O(N^2) = O(TN^2)$. Since $T \ll N^2$ in our case, the overall time complexity is $O(N^2)$. This is consistent with most graph diffusion models [31, 39, 49] and robust GNNs [13, 26, 67].

D Experiment Details

D.1 Dataset Details

D.1.1 Graph Classification Datasets. We use the following five real-world datasets to evaluate the robustness of DiffSP on the graph classification task. All the dataset is obtained from PyG TUDataset²

- **MUTAG** [24] contains graphs of small molecules, with nodes as atoms and edges representing chemical bonds. Labels indicate molecular toxicity.
- **IMDB-BINARY** [24] consists of movie-related graphs, where nodes are individuals, and edges represent relationships. Labels classify the movie as Action or Romance.
- **IMDB-MULTI** [24] is similar, but edges connect nodes across three genres: Comedy, Romance, and Sci-Fi, with corresponding labels.
- **REDDIT-BINARY** [24] features user discussion graphs from Reddit, with edges indicating responses. Graphs are labeled as either question-answer or discussion-based.

² https://pytorch-geometric.readthedocs.io/en/latest/generated/torch_geometric.datasets.TUDataset.html

Table D.1: Statistics for graph classification datasets

Dataset	#graph	#avg. node	#avg. edge	#feature	#class
MUTAG	188	17.9	39.6	7	2
IMDB-BINARY	100	19.8	193.1	/	2
IMDB-MULTI	1500	13.0	65.9	/	3
REDDIT-BINARY	2000	429.6	995.5	/	2
COLLAB	5000	74.5	4914.4	/	2

Table D.2: Statistics for node classification datasets

Dataset	#node	#edge	#feature	#class
Cora	2708	10556	1433	7
CiteSeer	3327	9104	3703	2
PolBlogs	1490	19025	/	2
Photo	7487	119043	745	8

- **COLLAB** [24] consists of collaboration networks, where nodes are researchers, and edges represent collaborations. Labels identify the research field: High Energy Physics, Condensed Matter Physics, or Astro Physics.

Statistics of the graph classification datasets are in Table D.1.

D.1.2 Node Classification Datasets. We use the following four real-world datasets to evaluate the robustness of DiffSP on the node classification task.

- **Cora** [59] is a citation network where nodes represent publications, with binary word vectors as features. Edges indicate citation relationships.
- **CiteSeer** [59] is another citation network, similar to Cora, with nodes representing research papers and edges denoting citation links.
- **PolBlogs** [1] is a political blog network, where edges are hyperlinks between blogs. Nodes are labeled by political affiliation: liberal or conservative.
- **Photo** [41] is a co-purchase network from Amazon, where nodes are products, edges represent frequent co-purchases, and features are bag-of-words from product reviews. Class labels indicate product categories.

The statistics of the graph classification datasets are given in Table D.2. Cora and CiteSeer is obtained from PyG Planetoid³. PolBlogs is obtained from PyG PolBlogs⁴. Photo is obtained from PyG Amazon⁵.

D.2 Description of Baselines

D.2.1 Graph Classification Baselines.

- **IDGL** [9] iteratively refines graph structures and embeddings for robust learning in noisy graphs.
- **GraphCL** [60] maximizes agreement between augmented graph views via contrastive loss.
- **VIB-GSL** [47] applies the Information Bottleneck to learn task-relevant graph structures.
- **G-Mixup** [20] generates synthetic graphs by mixing graphons to enhance generalization.

³ https://pytorch-geometric.readthedocs.io/en/latest/generated/torch_geometric.datasets.Planetoid.html#torch_geometric.datasets.Planetoid

⁴ https://pytorch-geometric.readthedocs.io/en/latest/generated/torch_geometric.datasets.PolBlogs.html#torch_geometric.datasets.PolBlogs

⁵ https://pytorch-geometric.readthedocs.io/en/latest/generated/torch_geometric.datasets.Amazon.html#torch_geometric.datasets.Amazon

- **SEP** [53] minimizes structural entropy for optimized graph pooling.
- **MGRL** [36] addresses semantic bias and confidence collapse with instance-view consistency and class-view learning.
- **SCGCN** [68] ensures robustness with temporal and perturbation stability.
- **HGP-SL** [65] combines pooling and structure learning to preserve key substructures.
- **SubGatPool** [4] uses subgraph attention and hierarchical pooling for robust classification.
- **DIR** [55] identifies stable causal structures via interventional separation.
- **VGIB** [61] filters irrelevant nodes through noise injection for improved subgraph recognition.

In our implementation, since the authors of MGRL and SubGatPool have not provided open access to their code, we reproduced their methods based on the descriptions in their papers. The implementations of other baselines can be found at the following URLs:

- **IDGL**: <https://github.com/hugochan/IDGL>
- **GraphCL**: <https://github.com/Shen-Lab/GraphCL>
- **VIB-GSL**: <https://github.com/VIB-GSL/VIB-GSL>
- **G-Mixup**: <https://github.com/ahxt/g-mixup>
- **SEP**: <https://github.com/Wu-Junran/SEP>
- **SCGCN**: <https://github.com/DataLab-atom/temp>
- **HGP-SL**: <https://github.com/cs Zhangzhen/HGP-SL>
- **DIR**: <https://github.com/Wuyxin/DIR-GNN>
- **VGIB**: <https://github.com/Samyu0304/VGIB>

D.2.2 Node Classification Baselines.

- **GSR** [67] refines graph structures via a pretrain-finetune pipeline using multi-view contrastive learning to estimate and adjust edge probabilities.
- **GARNET** [11] improves GNN robustness by using spectral embedding and probabilistic models to filter adversarial edges.
- **GUARD** [29] creates a universal defensive patch to remove adversarial edges, providing node-agnostic, scalable protection.
- **SVDGCN** [13] applies Truncated SVD preprocessing with a two-layer GCN.
- **JaccardGCN** [52] drops dissimilar edges in the graph before training a GCN.
- **RGCN** [70] models node features as Gaussian distributions, using variance-based attention for robustness.
- **Median-GCN** [6] improves robustness by using median aggregation instead of the weighted mean.
- **GNNGuard** [64] defends GNNs by pruning suspicious edges through neighbor importance estimation.
- **SoftMedian** [17] filters outliers by applying a weighted mean based on distance from the median to defend against adversarial noise.
- **ElasticGNN** [34] combines 1-based and 2-based smoothing, balancing global and local smoothness for better defense.
- **GraphADV** [58] boosts robustness through adversarial training with gradient-based topology attacks.

The implementations of these node classification baselines can be found at the following URLs:

- **GSR**: <https://github.com/andyjzhao/WSDM23-GSR>
- **GARNET**: <https://github.com/cornell-zhang/GARNET>
- **GUARD**: <https://github.com/EdisonLeeeee/GUARD>
- **SVD**: https://github.com/DSE-MSU/DeepRobust/blob/master/deeprobust/graph/defense/gcn_preprocess.py
- **Jaccard**: https://github.com/DSE-MSU/DeepRobust/blob/master/deeprobust/graph/defense/gcn_preprocess.py
- **RGCN**: https://github.com/DSE-MSU/DeepRobust/blob/master/deeprobust/graph/defense/r_gcn.py
- **Median-GCN**: https://github.com/DSE-MSU/DeepRobust/blob/master/deeprobust/graph/defense/median_gcn.py
- **GNNGuard**: <https://github.com/mims-harvard/GNNGuard>
- **SoftMedian**: https://github.com/sigeisler/robustness_of_gnns_at_scale
- **ElasticGCN**: <https://github.com/lxiaorui/ElasticGNN>
- **GraphADT**: https://github.com/KaidiXu/GCN_ADV_Train

D.3 Attack Setting Details

D.3.1 Graph Classification Attack Settings. For graph classification attacks, we use the following three attack methods:

- **GradArgmax** [10] greedily selects edges for perturbation based on the gradient of each node pair.
- **PR-BCD** [17] performs sparsity-aware first-order optimization attacks using randomized block coordinate descent, enabling efficient attacks on large-scale graphs.
- **CAMA-Subgraph** [51] enhances adversarial attacks in graph classification by targeting critical subgraphs. It identifies top-ranked nodes via a Class Activation Mapping (CAM) framework and perturbs edges within these subgraphs to craft more precise adversarial examples.

Note that, as the authors of CAMA-Subgraph have not provided open access to their code, we reproduced their method based on the descriptions in their papers. The reproduced code is available in our repository. For the implementation of other baselines, we used code from the following URLs:

- **GradArgmax**: https://github.com/xingchenwan/grabnel/blob/main/src/attack/grad_arg_max.py
- **PR-BCD**: https://github.com/pyg-team/pytorch_geometric/blob/master/torch_geometric/contrib/nn/models/rbcd_attack.py

For all graphs in the dataset, we set 20% of the total number of edges as the attack budget. We use a two-layer GCN followed by a mean pooling layer and a linear layer as the surrogate model, which shares the same architecture as the classifier for all baselines.

D.3.2 Node Classification Attack Settings. For targeted node classification attacks, we use the following three attack methods:

- **PR-BCD** [17] performs the same attack as in graph classification but targets a different task.
- **Nettack** [71] incrementally modifies key edges or features to maximize the difference in log probabilities between correct and incorrect classes, while preserving the graph’s core properties, such as the degree distribution.
- **GR-BCD** [17] is similar to PR-BCD but flips edges greedily based on the gradient concerning the adjacency matrix.

The implements of these attacks can be found from the following URLs:

- **PR-BCD**: https://github.com/pyg-team/pytorch_geometric/blob/master/torch_geometric/contrib/nn/models/rbcd_attack.py
- **Nettack**: https://github.com/DSE-MSU/DeepRobust/blob/master/deeprobust/graph/targeted_attack/nettack.py
- **GR-BCD**: https://github.com/pyg-team/pytorch_geometric/blob/master/torch_geometric/contrib/nn/models/rbcd_attack.py

For all datasets, we set 10% of the total number of edges as the attack budget for both PR-BCD and GR-BCD. For Nettack, following the settings from deeprobust [32], we select 40 nodes from the test set to attack with a budget of 5 edges and evaluate accuracy. These 40 nodes include 1) 10 nodes with the highest classification margin (clearly correctly classified), 2) 10 nodes with the lowest margin (still correctly classified), and 3) 20 randomly selected nodes.

For non-targeted node classification attacks, we use the following three attack methods:

- **MinMax** [32] generates adversarial perturbations by solving a min-max optimization. The outer step finds optimal edge perturbations, while the inner step retrains the GNN to adapt.
- **DICE** [72] removes edges between same-class nodes and inserts edges between nodes of different classes.
- **Random** [32] randomly adds edges to the input graph.

The implements of these attacks can be found in the following URLs:

- **MinMax**: https://github.com/DSE-MSU/DeepRobust/blob/master/deeprobust/graph/global_attack/topology_attack.py
- **DICE**: https://github.com/DSE-MSU/DeepRobust/blob/master/deeprobust/graph/global_attack/dice.py
- **Random**: https://github.com/DSE-MSU/DeepRobust/blob/master/deeprobust/graph/global_attack/random_attack.py

For MinMax, DICE, and Random attacks, we set the attack budget to 10%, 20%, and 30% of the total number of edges, respectively, for all datasets.

D.4 Implement Details

For graph classification, we randomly split the dataset into 8:1:1 for training, validation, and testing. For datasets without node features, we use normalized node degrees as features, following the approach in [47]. The testing set is subjected to adversarial attacks. Our classifier consists of a two-layer Graph Convolutional Network (GCN) followed by a mean pooling layer and a linear layer. Both the diffusion model of DiffSP and the classifier are trained on the training graphs, with their performance evaluated on the attacked testing set. For node classification, we use the transductive setting with a 1:1:8 random split for training, validation, and testing. The classifier comprises a two-layer GCN followed by a linear layer. During training, we sample batches of subgraphs, consistent with [31], and apply adversarial attacks at test time. A learning rate of 0.0003 is used for all datasets. We perform 10 random runs for each method and report the average results. DiffSP is implemented in PyTorch with $\sigma = 2$ and $\alpha = 2$. Additional important parameter values are provided in Table D.3. More implement detailed information is available at <https://anonymous.4open.science/r/DiffSP>.

All the experiments were conducted on an Ubuntu 20.04 LTS operating system, utilizing an Intel Xeon Platinum 8358 CPU (2.60GHz)

Table D.3: Hyperparameter settings

Hyperparameter	MT	IB	IM	RB	CL	Cora	CiteSeer	PolBlogs	Photo
k	4	6	6	8	8	7	8	8	8
λ	1e1	1e2	1e3	1e3	1e3	1e3	1e3	1e3	1e3
purification steps	4	6	5	6	4	6	6	6	6

with 1TB DDR4 RAM. For GPU computations, an NVIDIA Tesla A100 SMX4 with 40GB of memory was used.

E Limitations and Future Discussions

Although DiffSP enhances the robustness of graph learning against evasion attacks through prior-free structure purification, it still has certain limitations, which we aim to address in future work. Specifically: 1) In addition to structural disturbances, feature perturbations are common in real-world scenarios. In future steps, we plan to incorporate experiments on feature-based attacks and evaluate robustness in link prediction tasks under evasion attacks. 2) Estimating the adversarial degree of nodes is crucial for non-isotropic noise injection. We aim to develop a more accurate estimation method to further enhance the robustness of graph learning. 3) We also plan to optimize the time complexity of DiffSP to make it more efficient.

Furthermore, the graph entropy estimation approach proposed in this work is a promising tool. We will explore ways to enhance the properties encapsulated by graph entropy, such as designing better Z to capture the more local structure and feature characteristics of nodes. Additionally, we plan to utilize this graph entropy method to further investigate graph properties across diverse scenarios, facilitating more extensive research in this area.